CANADIAN THESES

THÈSES CANADIENNES

NOTICE

AVIS

Canadä

CANADIAN THESES ON MICROFICHE SERVICE – SERVICE DES THÈSES CANADIENNES SUR MICROFICHE

PERMISION TO MICROFILM – AUTORISATION DE MICROFILMER

• Please print or type – Écrire en lettres moulées ou dactylographier

AUTHOR – AUTEUR

Full Name of Author – Nom complet de l'auteur

Kort Paul, Ratzlaff

Date of Birth – Date de naissance

Feb. 17, 1955

Canadian Citizen – Citoyen canadien

☑ Yes / Oui ☐ No / Non

Country of Birth – Lieu de naissance

Canada

Permanent Address – Residence fixe

*5504 Centre St. N
Calgary, Alberta, Canada
T2K 0T3*

THESIS – THÈSE

Title of Thesis – Titre de la thèse

*Behaviour and Ultimate Strength of Transversely
Loaded Continuous Steel Plates*

Degree for which thesis was presented
Grade pour lequel cette thèse fut présentée

M.Sc.

Year this degree conferred
Année d'obtention de ce grade

1985

University – Université

University of Alberta

Name of Supervisor – Nom du directeur de thèse

Dr. D J L. Kennedy

AUTHORIZATION – AUTORISATION

Permission is hereby granted to the NATIONAL LIBRARY OF CANADA to **microfilm** this thesis and to **lend** or **sell copies of the film.**

The author reserves other publication rights, and neither the thesis nor extensive extracts from it may be printed or otherwise reproduced without the author's written permission.

L'autorisation est, par la présente, accordée à la BIBLIOTHÈQUE NATIONALE DU CANADA de **microfilmer** cette thèse et de **prêter** ou de **vendre des exemplaires du film.**

L'auteur se réserve les autres droits de publication; ni la thèse ni de longs extraits de celle-ci ne doivent être imprimés ou autrement reproduits sans l'autorisation écrite de l'auteur.

▶ ATTACH FORM TO THESIS – VEUILLEZ JOINDRE CE FORMULAIRE À LA THÈSE ◀

Signature

Date

Oct. 11/85

NL-91 (r 84/03)

Canada

THE UNIVERSITY OF ALBERTA

BEHAVIOUR AND ULTIMATE STRENGTH OF TRANSVERSELY LOADED
CONTINUOUS STEEL PLATES

by

© KURT PAUL RATZLAFF

A THESIS

SUBMITTED TO THE FACULTY OF GRADUATE STUDIES AND RESEARCH
IN PARTIAL FULFILMENT OF THE REQUIREMENTS FOR THE DEGREE
OF MASTER OF SCIENCE

DEPARTMENT OF CIVIL ENGINEERING

EDMONTON, ALBERTA

FALL 1985

THE UNIVERSITY OF ALBERTA

RELEASE FORM

NAME OF AUTHOR   KURT PAUL RATZLAFF

TITLE OF THESIS   BEHAVIOUR AND ULTIMATE STRENGTH OF

TRANSVERSELY LOADED CONTINUOUS STEEL

PLATES

DEGREE FOR WHICH THESIS WAS PRESENTED MASTER OF SCIENCE

YEAR THIS DEGREE GRANTED   FALL 1985

Permission is hereby granted to THE UNIVERSITY OF

ALBERTA LIBRARY to reproduce single copies of this

thesis and to lend or sell such copies for private,

scholarly or scientific research purposes only.

The author reserves other publication rights, and

neither the thesis nor extensive extracts from it may

be printed or otherwise reproduced without the author's

written permission.

(SIGNED) ....

PERMANENT ADDRESS:

...5504 Centre Str. N.

...Calgary, Alberta...

...Canada,.......T2K 0T3

DATED ...Oct. 9......19 85

THE UNIVERSITY OF ALBERTA

FACULTY OF GRADUATE STUDIES AND RESEARCH

The undersigned certify that they have read, and
recommend to the Faculty of Graduate Studies and Research,
for acceptance, a thesis entitled BEHAVIOUR AND ULTIMATE
STRENGTH OF TRANSVERSELY LOADED CONTINUOUS STEEL PLATES
submitted by KURT PAUL RATZLAFF in partial fulfilment of the
requirements for the degree of MASTER OF SCIENCE.

....

Supervisor

....

....

....

Date...October 9, 1985....

ABSTRACT

An initially flat rectangular steel plate, clamped on all four sides against rotation and translation, displays three modes of behaviour as the intensity of a uniform transverse load increases. These modes are described as elastic flexural-membrane behaviour, inelastic flexural-membrane action and inelastic membrane action.

For a long narrow plate, elastic flexural-membrane action exists up to the load causing yielding of the extreme fibres along the long edges on the loaded face. Subsequent plastic hinge formation along the long edges reduces the stiffness. Inelastic flexural-membrane action ends with complete yielding in tension along the long edges. The plate then acts essentially as a membrane straining inelastically as yielding gradually progresses from both edges toward the centre. A lower bound to this behaviour is obtained by assumming that Poisson's ratio is the elastic value and the maximum membrane stress is the yield stress. A higher lower bound is obtained by using the plastic value of Poisson's ratio. An analysis culminating with inelastic membrane action taking into account the stress-strain relationship beyond yielding is proposed. This analysis shows that the load deflection curve gradually moves above the lower bounds because the edge forces can exceed yield.

A finite element program modelling uniaxial plane strain conditions, the inelastic Poisson's ratio and the stress-strain behaviour to failure gave a load-deflection response closely following the three predicted regions of behaviour. Two failure criteria related to local edge

iv

conditions have been established; a limiting tensile strain due to bending and tension and the edge shear resistance. The behaviour and failure loads have been confirmed by two tests. Strain measurements taken during the tests substantiate in general the predicted behaviour.

Implications for using the ultimate strength of continuous steel plates for the design of offshore structures for oil exploration and production in the Arctic are presented.

ACKNOWLEDGEMENTS

Table of Contents

List of Tables

List of Figures

List of Symbols

A_b =   cross-sectional area of one bolt based on the nominal diameter

A_f =   area of fractured surface

A_i =   net cross-sectional area at time t=i

A_o =   net cross-sectional area at time t=0

d =   distance from the centre of curvature at the plate edge to the nearest point on the plate where the curvature is zero, at the midsurface

D =   flexural rigidity $= Eh^3/12(1-\nu^2)$

e =   eccentricity

E =   modulus of elasticity

F_u =   ultimate uniaxial tensile strength

h =   plate thickness

ℓ =   length

L =   plate width between supports

M =   bending moment per unit length

M_o =   bending moment per unit length at plate edge

Mp =   fully plastic moment per unit length $= \sigma_y h^2/4$

Mu   =   ultimate plastic moment per unit length = $\sigma_u h^2/4$

My   =   yield moment per unit length

N_x =   membrane force in x direction per unit length

P   =   component of membrane force S per unit length

P_o =   axial component of membrane force per unit length at plate edge

Pu   =   ultimate axial force per unit length

q   =   uniform load per unit area

q_c =   critical uniform load per unit area = $16Mp/L^2$

S   =   axial membrane force per unit length

S_y =   membrane yield force per unit length

T   =   applied transverse load

U   =   membrane stress parameter = $[SL^2/4D]^{1/2}$

V   =   coefficient of variation

V_o =   transverse shear force per unit length at plate edge

w   =   deflection

W_{max} =   midspan deflection

$(W_{max})_y$ = midspan deflection at yield load

$x, y, z,$ = cartesian coordinates

a = angle in degrees

β = aspect ratio of plate, width/length

δ = volume change

ϵ = strain

ϵ_f = true fracture strain

ϵ_i = true strain at time i

ϵ_p, ϵ_s = true axial strain

ϵ_{st} = strain-hardening strain

ϵ_u = ultimate strain

ϵ_y = yield strain

λ = elongation

ν = Poisson's ratio in the elastic range = 0.3

ν_p = Poisson's ratio in the inelastic range = 0.5

ν_s = effective Poisson's ratio of membrane

ϕ = dw^2/dx^2 = curvature

ϕ_y = curvature corresponding to My

π = a constant, 3.1416

ρ_c = critical radius of curvature

ρ_{min} = minimum radius of local curvature

σ_e = effective stress

σ_s = axial membrane stress

σ_u = ultimate strength in uniaxial tension

σ_y = yield stress in uniaxial tension

σ_X = normal stress parallel to X axis

σ_Y = normal stress parallel to Y axis

τ_u = ultimate shear strength

τ_{XY} = shear stress on X-Y plane

θ = edge inclination in degrees

1. INTRODUCTION

1.1 Scope and Objectives

The overall objective of this research is to provide analyses that predict accurately the load-deflection response of transversely loaded continuous steel plates, including the failure mode and load, and to confirm the analyses by test. In this work only long plates with aspect ratios approaching zero have been considered.

1.2 General

In the design of flat plate floors the limit of structural usefulness is generally considered to be the flexural strength of the plate system. In some cases the flexural strength may be even limited to that based on elastic behaviour, neglecting the considerable strength beyond first yield until a failure mechanism develops. Classical yield-line theory determines this latter load carrying capacity. Such limits are irrelevant for any system in which the deflections are not critical and in which the increase in strength due to membrane action can be considered.

Membrane action develops as the plate deforms and transverse loads are carried by in-plane tensile stresses. The two-way membrane action in a plate is analogous to the one-way action of a cable supporting transverse loads. Furthermore, for steel plates that are continuous over a

rectangular grid of beams and stiffeners, such as in a caisson type structure, full advantage can be taken of the ductility of the steel and the increased load carrying capacity of the membrane in the inelastic range. The load carrying capacity may be many times that predicted on the basis of flexural action alone and still provide any desired level of safety.

Some of the structures that have been designed or proposed for oil exploration and production in the Arctic Ocean consist of steel caissons formed from continuous plating supported laterally by a rectangular grid of stiffeners, beams and girders. Interior rectangular plate panels are continuous over the supports on all four edges and can therefore be modelled as being restrained against rotation and translation along all edges. Under the action of floe ice the steel plates are subjected to enormous forces. The economic design of such structures requires, therefore, that the full strength of the plates be mobilized. Before design procedures can be developed for this and other applications a comprehensive method of analysis is needed to describe the complete behaviour of the plates into the inelastic range, including the failure mode and load.

An extensive literature survey has been carried out and relevant experimental data have been reviewed. Based on this review and an examination of the limits of behaviour, a method of analysis is proposed that considers inelastic

membrane behaviour. Two failure criteria have been established and the results of two computer simulations using a finite element method are reported. The results of two tests on plates subjected to fluid pressure and with an aspect ratio of 1/3, are reported.

2. LITERATURE REVIEW

2.1 General

Literature on continuous steel plates acted upon by transverse loads has been primarily concerned with closed-form mathematical solutions to define precisely the elastic and elasto-plastic load-deflection response and with permanent inelastic deformations. The inelastic deformations of a steel plate ship hull, for example, either due to normal operations or collisions, remains an important design criterion for naval architects. However, the complexities involved in modelling mathematically inelastic plate behaviour has prohibited exactness among the numerous solutions proposed because of the introduction of simplifying assumptions. The result is that designers of flat plate structures have to estimate behaviour and deformations and, presumeably, ultimate strengths.

Generally, an inelastic large deflection analysis must include:

(i) both elastic and inelastic material properties,

(ii) changing plate geometry with loading, including

(iii) elastic and inelastic deflections, and

(iv) load type and location.

Differential equations describing the large deflection elastic behaviour of uniformly transversely loaded clamped rectangular flat steel plates of any aspect ratio were first derived by von Karman in 1910. Earlier, Boobnoff (1902) had

4

determined the exact solution for an infinitely long plate (one with an aspect ratio, width/length, of zero).

For an infinitely long flat plate the von Karman equations, when shear deformations are neglected, reduce to

$$[2.1] \qquad \frac{q}{D} = \frac{d^4w}{dx^4} - \frac{N_x}{D}\frac{d^2w}{dx^2}$$

Furthermore, if the term containing the membrane force N_x in [2.1] is neglected, the equation reduces to the elastic small deflection equation of Lagrange. Some approximate solutions to the large deflection equations of von Karman for rectangular plates were first presented by Way (1938). Levy (1942) used a Fourier series method to solve the same equations for a plate with an aspect ratio of 1. To the author's knowledge, no closed-form solution to the complete von Karman equations exists for a plate with an aspect ratio other than zero. Approximate solutions abound for the inelastic behaviour of transversely loaded plates when the plate material is assumed to exhibit elasto-plastic behaviour. These solutions are generally considered too mathematically rigorous for use in design.

In the design of continuous plating supported by a rectangular grid of beams and stiffeners it may be assumed that the entire resistance to lateral loads results from flexural action only. This analysis may be further limited

to elastic behaviour and is considered valid to use for design only if it is necessary to limit deflections and ensure elastic behaviour of the plate. Although plates with a large span to thickness ratio, say 100, have negligible bending resistance they can carry large transverse loads primarily through membrame action.

For a strip of flat plate one unit wide as shown in Fig. 2.1, taken from a plate with an aspect ratio of zero, when the stress-strain relationship is assumed to be elasto-plastic as shown in Fig. 2.2 the uniform transverse collapse load as given by numerous authors is

$$[2.2] \qquad q = \frac{16\ Mp}{L^2}$$

The strip is fixed rotationally at the edges but one edge may move towards the other.

If it is assumed, according to the maximum principal strain theory, that yielding occurs when the strain reaches the uniaxial yield strain and considering the fact that the plate strip is two-dimensional, resulting in a biaxial stress or uniaxial plane strain condition (Lay, 1982), the fully plastic moment per unit width is determined to be

$$[2.3] \qquad Mp = \frac{\sigma_y\ h^2}{4(1-\nu^2)}$$
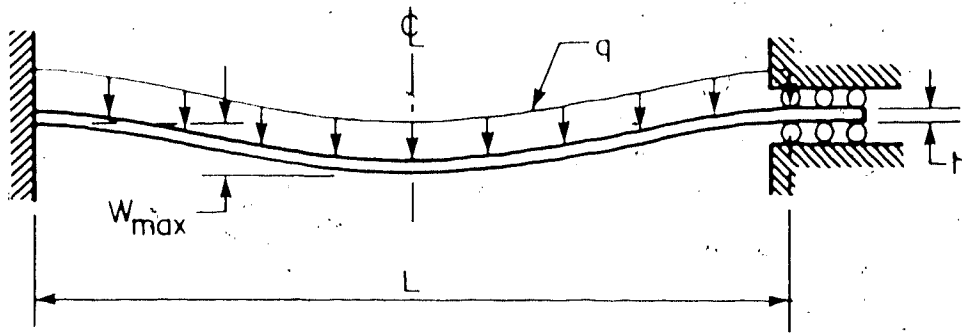
Figure 2.1 Transversely loaded plate in flexure
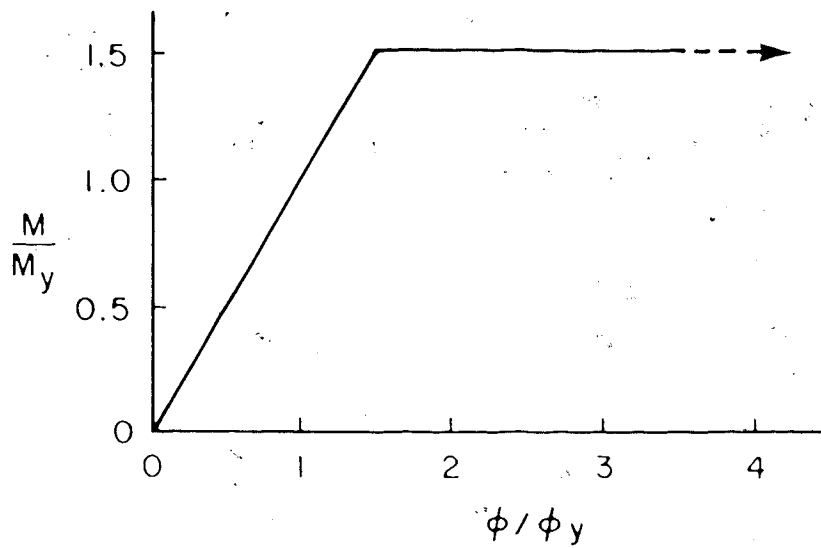
Figure 2.2 Elasto-plastic moment-curvature relationship

The maximum principal strain yield criterion gives, under a condition of biaxial tension, an equivalent yield stress equal to $\sigma_y/(1-\nu^2)$. This criterion gives a yield strength 2 percent higher than that using the von Mises maximum energy of distortion theory when Poisson's ratio, ν, is equal to 0.3. For structural steels, an appropriate value of Poisson's ratio in the elastic range is about 0.3 (Clarkson, 1956; Lay, 1982). Once yielding occurs, and significant portions of the cross-section at the hinge locations have been strained inelastically, the appropriate value of Poisson's ratio to be used is ν_p, the inelastic value. The inelastic value is commonly taken as 0.5, implying that zero volume change occurs in the yielding process, which is consistent with the fact that yielding occurs because of shear distortions. Therefore, substituting [2.3] in [2.2] and using the appropriate inelastic value of Poisson's ratio, the critical uniform transverse load causing a collapse mechanism is found to be

$$[2.4] \qquad q_c = \frac{4\,\sigma_y}{(1-\nu_p^2)}\left[\frac{h}{L}\right]^2$$

The respective upper and lower bound uniformly distributed collapse load for a rigidly clamped rectangular plate given by Jones (1976) and numerous other authors are

$$[2.5] \qquad q_c = \frac{48\ Mp}{L^2(\sqrt{3 + \beta^2} - \beta)^2}$$

and

$$[2.6] \qquad q_c = \frac{16Mp}{L^2}(1 + \beta^2)$$

respectively, where β is equal to the aspect ratio, width/length. With β equal to zero, [2.5] and [2.6] are identical and equal to [2.2].

The load-deflection behaviour based on the flexural analysis described above, for a plate with L/h equal to 80 and an aspect ratio of zero, as presented in Fig. 2.3. in nondimensionalized form, consists of three straight lines. The first portion gives the flexural deflection until hinges form at the edges. The second portion, with 1/5 the slope, gives the increasing deformation occuring as the plate deflects with zero rotational restraint and constant moment at the edges. When the collapse load, q_c, is reached, a mechanism has formed and the plate deflects without limit.
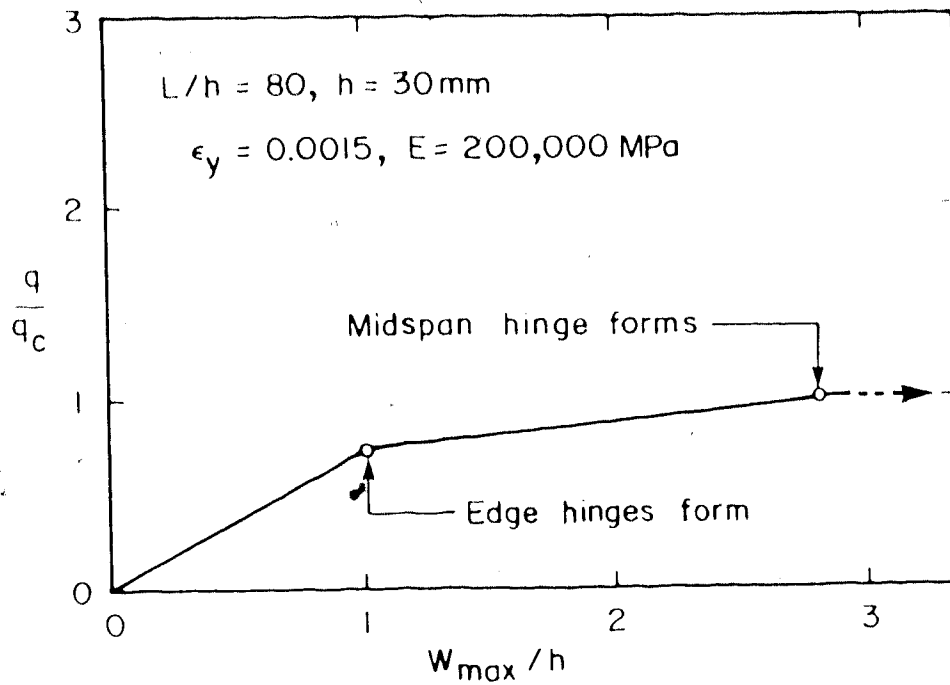
Figure 2.3 Load-deflection behaviour in flexure
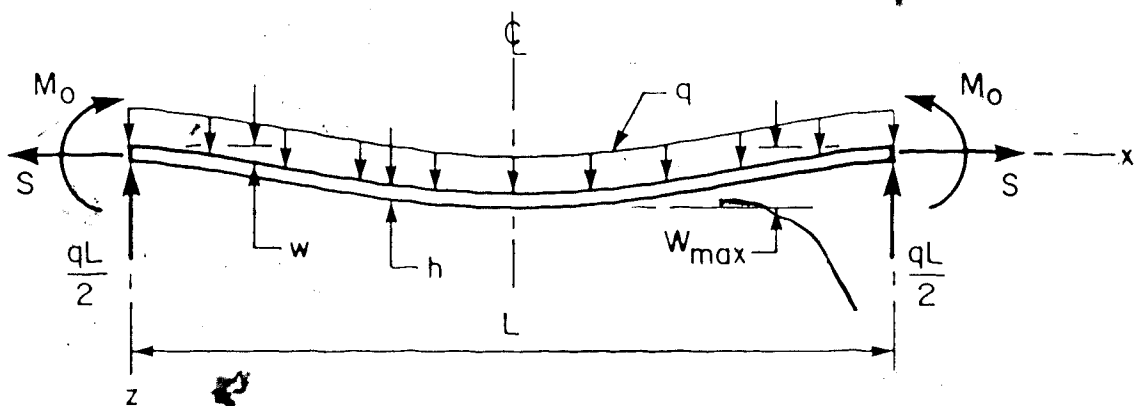
Figure 2.4 Free body diagram of plate with full edge restraint

2.2 Timoshenko (1940)

Timoshenko considered a strip of an infinitely long plate with an aspect ratio of zero as shown in Fig. 2.4. The edges are restrained rotationally and translationally and upon the application of load give rise there to bending moments Mo and membrane forces S. The midspan or maximum deflection, also shown in Fig. 2.4, is W_{max} while the deflection at any position x along the plate length is w. At any cross-section of the uniformly loaded plate the bending moment is

$$[2.7] \quad M(x) = \frac{q}{2}(Lx - x^2) - Sw + Mo$$

Under uniaxial plane strain conditions, the moment-curvature relationship for the rectangular cross-section is

$$[2.8] \quad D\frac{d^2w}{dx^2} = -M(x)$$

where D is equal to the flexural rigidity, $Eh^3/12(1-\nu^2)$. Substituting [2.8] in [2.7] results in

$$[2.9] \quad \frac{d^2w}{dx^2} + \frac{Sw}{D} = \frac{q}{2D}(Lx - x^2) + \frac{Mo}{D}$$

With the boundary conditions:

$$(i) \quad \frac{dw}{dx} = 0 \quad (\text{at } x = 0 \text{ and } x = L/2)$$

$$(ii) \quad w = 0 \quad (\text{at } x = 0)$$

the solution to [2.9] is

$$[2.10] \quad w = \frac{qL^4}{16u^3 D \tanh U}\left[\frac{\cosh[U(1 - 2x/L]}{\cosh U} - 1\right]$$

$$+ \frac{qL^2}{8U^2 D}(Lx - x)^2$$

where the membrane stress parameter, U, is given as

$$[2.11] \quad U = \sqrt{\frac{SL^2}{4D}}$$

The deflections given by [2.10] are, as would be expected, a function of the membrane force, S. If the deflections are assumed to be small relative to the width of the plate, L, the extension of the centreline of the loaded strip can be taken as

$$[2.12] \qquad \lambda = \int_{0}^{L/2} \left[\frac{dw}{dx}^2 \right] dx$$

Assuming that the average membrane strain is λ/L, the membrane force at the edges becomes

$$[2.13] \qquad S = \frac{\lambda E h}{L(1 - \nu^2)}$$

By differentiating [2.10] with respect to x and substituting the result into [2.12], the following expression for computing U is found:

$$[2.14] \qquad \frac{E^2 h^8}{q^2 L^8 (1 - \nu^2)^2} = - \frac{81}{16U^7 \tanh U} - \frac{27}{16U^6 \sinh U} + \frac{27}{4U^8} + \frac{9}{8U^6}$$

U in [2.14] may be found by trial and error for a given load q and L/h ratio. The corresponding deflections are then determined using [2.10]. The resulting load-deflection

response from the analysis presented above for a plate with L/h=49.4, where h. = 0.93 mm, is shown in Fig. 2.5 as curve E. The uniformly distributed load q has been nondimensionalized by dividing by the collapse load q_c given by [2.4] and the maximum deflection W_{max} has been nondimensionalized by dividing by the plate thickness, h. In determining q, Poisson's ratio was taken as 0.3 as is appr   ate for steel in the elastic range.

The limit to Timoshenko's elastic analysis occurs when yielding begins at an extreme fibre in the plate, point A' on curve E of Fig. 2.5. This yielding occurs in tension at the edges on the loaded side of the plate where the bending moments are a maximum and where the tensile membrane force, S, causes additional tensile stresses. In the presence of the tensile membrane stresses the moment at first yield is less than My. If the moment-curvature relationship of the plate is assumed to be bilinear, up to the fully plastic moment Mp as shown in Fig. 2.2, the hinge at the edge of the plate forms fully and instantaneously at a moment less than the fully plastic moment due to the presence of tensile membrane forces, but at a moment greater than that corresponding to first yield with tensile forces present. The greater moment and resulting load carrying capacity corresponds to point A in Fig. 2.5 that lies considerably above point A' on curve E.

Also shown in Fig. 2.5 are the test results of Young (1959) for a plate with an aspect ratio of 1/3 and an L/h of
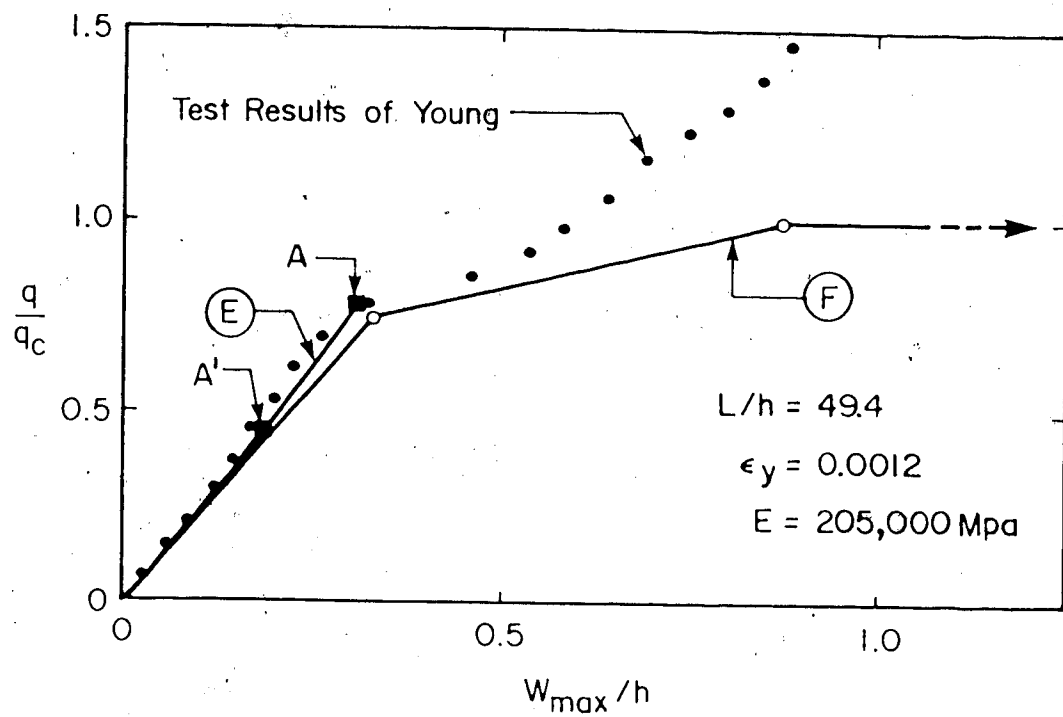
Figure 2.5 Load-deflection behaviour in flexure with and without membrane action

49.4. It is expected that the central, or maximum deflection of a plate with this aspect ratio would not be significantly different from that for a plate with an aspect ratio of zero (Clarkson, 1956; Hooke, 1970). Young's test results indicate that it is valid to consider the moment-curvature relationship to be elasto-plastic in Timoshenko's analysis as the results follow curve E to point A where the analysis assumes that hinges form instantaneously at the edges. Beyond point A the experimental data show that the stiffness of the plate deteriorates significantly and markedly.

The load-deflection response due to flexural action alone, shown in Fig. 2.5 as curve F, lies below that considering both flexural and membrane action, as would be expected. Where the load and corresponding deflection are approximately zero the slope of curves E and F are nearly identical. However, with increased loading, curve E lies above curve F showing that with membrane forces, for a given deflection, the load-carrying capacity is increased. It is expected that a greater increase in capacity would exist for plates having relatively larger L/h ratios, that is membrane action becomes relatively more important.

Timoshenko's elastic solution is the same as that obtained by the analytical perturbation method of Chien and Yeh (1957) as also used by Hooke (1969), when applied to the von Karman equations, applicable to plates with any aspect ratio, but used here for an aspect ratio of zero. Numerous other authors, both of textbooks and papers, have as well

presented numerical elastic and elasto-plastic solutions for transversely loaded plates taking into account both flexural and membrane behaviour. Timoshenko's closed-form solution for infinitely long plates confirms the iterative and numerical solutions proposed by others for plates with aspect ratios other than zero, up to the load corresponding to edge hinge formation.

2.3 Clarkson (1956)

The analysis presented by Clarkson considered both the elastic and inelastic performance of a transversely loaded, rigidly clamped, initially flat plate. Clarkson selected the convenient power series solution of Chien (1947) to solve the von Karman equations, applicable to plates of any aspect ratio, but used by him for an infinitely long plate with an aspect ratio of zero. The material was assumed to be homogeneous and isotropic with Hookean characteristics up to yield, with a modulus of elasticity modified by dividing by $1-\nu^2$ to take into account the biaxial stress field. Using the von Mises-Hencky yield criterion for the equivalent stress,

$$[2.15] \qquad \sigma_e = [\ \sigma_X^2 + \sigma_Y^2 - \sigma_X \sigma_Y + 3\tau_{XY}^2\ ]^{1/2}$$

yielding, in the principal direction of a biaxial stress

state, was taken to occur at a stress equal to

[2.16] $\sigma_p = \sigma_y / [1 - \nu + \nu^2]^{1/2}$

This criterion, based on the maximum distortion energy
theory, gives a tensile yield strength two percent higher
than that using the maximum principal strain theory when
Poisson's ratio is taken as 0.3. Clarkson assumed that
Poisson's ratio remained constant at a value of 0.3
throughout the elastic and plastic ranges and that the usual
bending theory of thin plates remained valid over the
load-deflection range considered. Three different solution
methods were established that covered the range between edge
hinge and midspan hinge formation. In the first method,
termed the complete elasto-plastic method, the change of
slope across the elasto-plastic zone of a hinge was found by
finite difference integration. In Clarkson's "corner yield"
method the width of the elasto-plastic strips at the edges,
which develop as load is increased, are ignored. Hinge
formation is assumed to occur when yielding is experienced
in the extreme tension fibres next to the loaded face at
plate boundaries and at the unloaded face at midspan. The
third, or 'plastic-hinge' method assumes instantaneous full
plastic hinge formation only after plasticity has spread
throughout the complete thickness of the plate. All of these

methods gave load deflection responses that were somewhat stiffer than the test results of Young (1959) and appear inapplicable when membrane action dominates.

Clarkson performed tests on 229 mm square plates with an L/h of 72. The plates did not, however, exhibit significant membrane action or increasing stiffness. Although Clarkson attempted to fix the edges of the plates, it is believed that there was a lack of membrane restraint. The results do, however, verify, up to the point just prior to midspan hinge formation, the extended elastic analysis of Timoshenko and Woinowsky-Krieger (1959) and the approximate plastic analysis of Jones and Walters (1971) for a plate with an aspect ratio of 1.

Clarkson presented design curves based on limiting the permanent deformation of the plate. The transverse load was restricted to that causing a plastic hinge to form at midspan or to that causing the membrane tension to reach two-thirds of the yield stress.

2.4 Young (1959)

Young (1959) investigated, both mathematically and experimentally, long rectangular plates (aspect ratio approaching zero), clamped at the edges and subject to uniform transverse loads, for the purpose of developing a plastic design method for ship plating. With shear and strain-hardening effects neglected, Young extended Timoshenko's elastic solution for infinitely long flat

plates beyond the formation of hinges at the edges to

midspan hinge formation. In this region of behaviour the

analysis assumed that:

(i) the material had elasto-plastic stress-strain

characteristics,

(ii) partial fixity existed at the edges for the

increment of load beyond the formation of the edge hinges,

(iii) the moment capacity deteriorated at the edge as

membrane forces increased,

(iv) the load carrying capacity increased until the

edge and centreline moments were equal, and

(v) yielding of the material occurred when the

effective stress corresponded to that given by [2.16].

The solution is iterative.

Young also presented an analysis for the

load-deflection behaviour beyond midspan hinge formation

based on various assumptions about the middle surface

strains at the plastic hinge locations - which are

apparently related to the membrane forces - and considered

the equilibrium of the membrane with both edge and midspan

hinges present. Unfortunately, as shown in Fig. 2.6, the

curve resulting from this analysis does not pass through the

point representing hinge formation at midspan found from the

iterative analysis. No explanation for this anomaly was

given.

Young also proposed a final limiting load-deflection

relationship that is reached when the entire cross-section
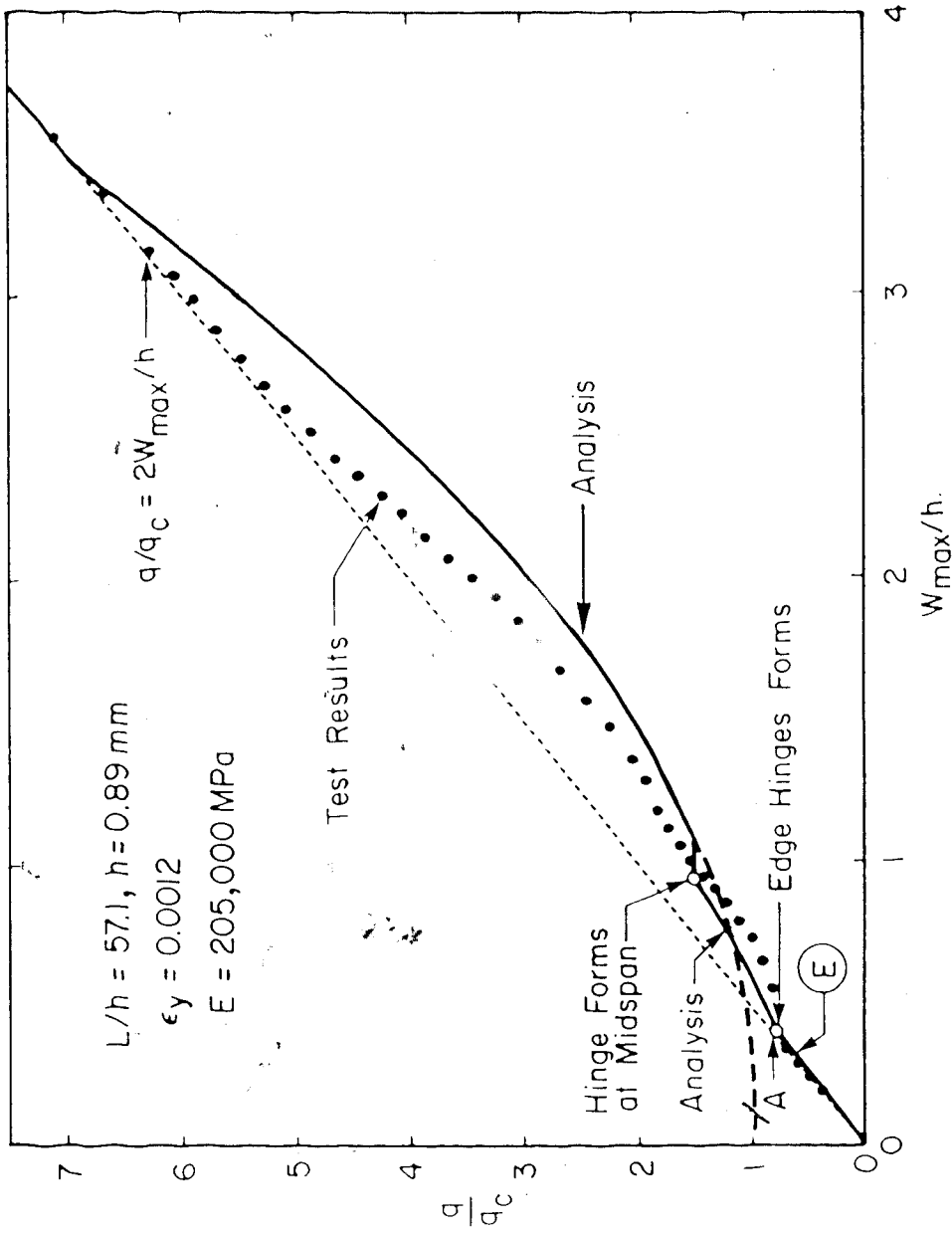
Figure 2.6 Analyses and test results of Young (1959)

of the plate is yielded in tension and no flexural action
remains. As shown in Fig. 2.6 this relationship is given by

$$[2.17] \qquad \frac{q}{q_c} = \frac{2W_{max}}{h}$$

Young did not consider the increasing inclination of the
membrane force at the edge as the membrane deflects nor
strain-hardening of the material. An effective Poisson's
ratio of 0.5 was used in this analysis.

The test values of Young shown in Fig. 2.6 agree well
with Timoshenko's analysis, curve E, up to point A but do
not coincide with the analyses that predict the load and
deflection corresponding to midspan hinge formation. They
do, however, finally approach the limiting straight line
given by [2.17].

2.5 Hooke (1970)

By using the Marguerre (1938) and von Karman equations
for initially deflected plates and flat plates respectively,
Hooke developed solutions similar to those of Nylander
(1951) for the post-elastic load-deflection behaviour of
uniformly transversely loaded rectangular plates, clamped at
all four edges. The solutions were an extension to that of
Clarkson (1956) who initially considered only infinitly long
flat plates. Good agreement exists between Hooke's analysis

and the **test results of** Hooke and Rawlings (1969) for plates

having **aspect ratios less** than 1/3. For plates having aspect

ratios **greater than about** 1/3 the load-deflection test

results of Hooke and Rawlings, and Clarkson, fall

considerably above Hooke's analysis and below his extended

elastic solution.

2.6 Fully Yielded Flexural-Membrane Behaviour

Kennedy and Hafez (1984) studied the behaviour of end

plate connections for steel beams in which the connection

consists simply of a rectangular steel plate welded at right

angles to the beam web and then bolted to a supporting

member. Some refinements to their analysis and further

design applications were presented by Kriviak and Kennedy

(1985). When the end of the beam rotates, the top of the end

plate is pulled transversely away from the supporting

member. In analysing this portion of the end plate

connection a 'T-section' was considered as shown in Fig.

2.7. Starting with the premise that plastic hinges due to

flexural action had already formed a mechanism (which

appears valid for the small L/h ratios of 11 and 22 in the

end plates), the expression derived for the applied force is

$$[2.18] \quad T = \frac{\ell S_y^2}{4Mp} \tan^2 a + \frac{4Mp}{\ell} \cos^2 a$$
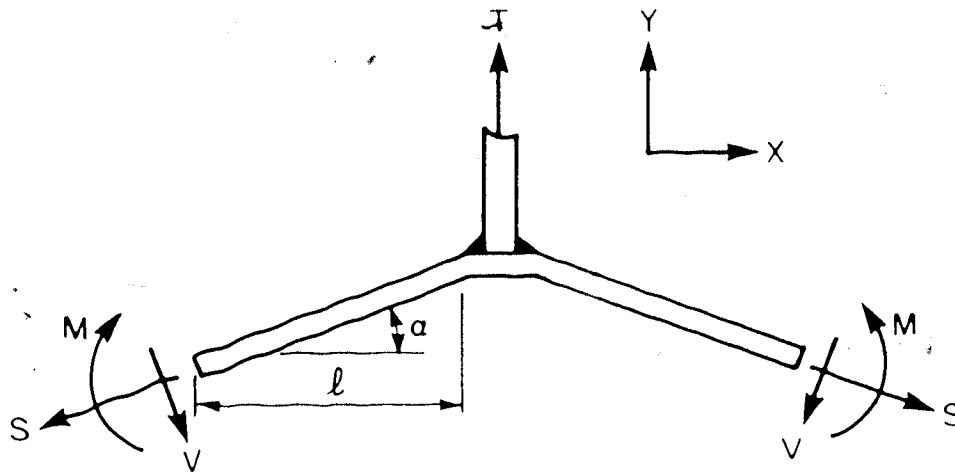
Figure 2.7 Free body diagram of T-section

$L/h = 80$, $h = 30\,mm$

$\epsilon_y = 0.0015$

$E = 200,000\,MPa$
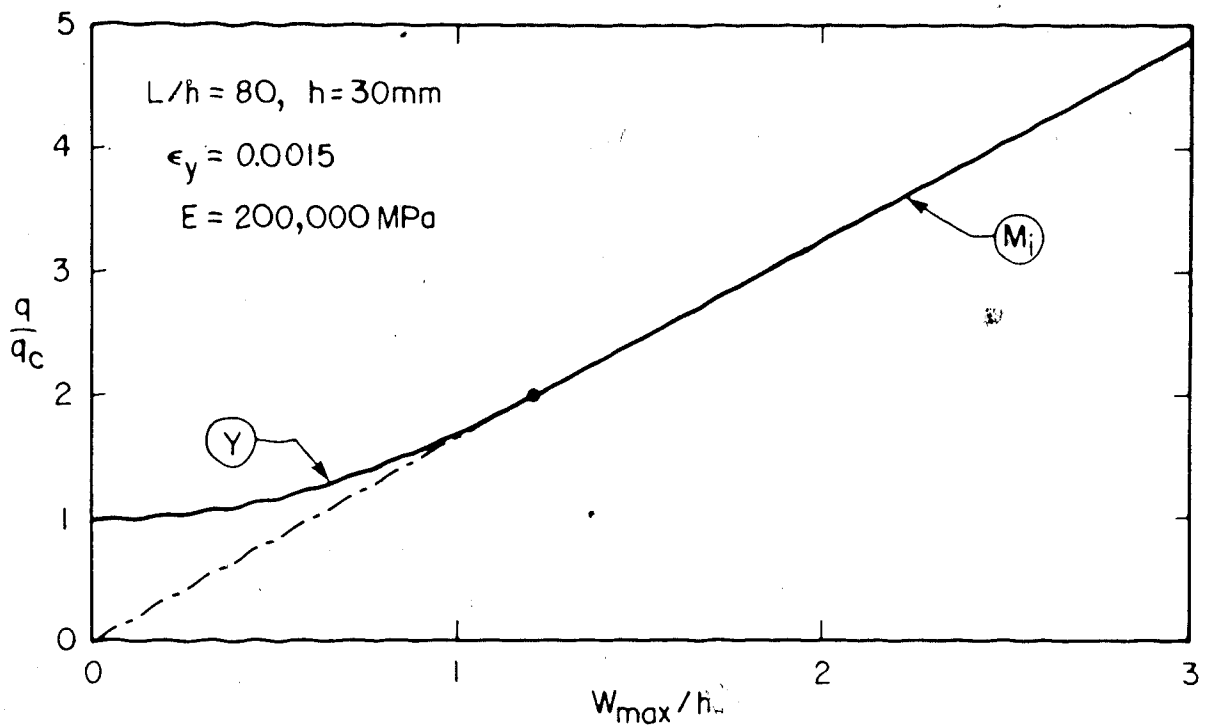
Figure 2.8 Load-deflection behaviour when fully yielded in flexure

This expression would be valid for a rectangular plate of zero aspect ratio, provided that the fully plastic moment is computed taking into account the uniaxial plane strain conditions.

Assuming that a uniform transverse load, q, rather than a line load, T, is acting on the mechanism that is fully yielded in flexure and that L is equal to 2ℓ, a summation of forces in the y direction gives

[2.19] $q = (2S \sin a)/L + (2V \cos a)/L$

Summing moments about one end of the plate gives

[2.20] $M = VL/(4 \cos a) - qL^2/16$

Rearanging [2.20] in terms of V and replacing V in [2.19] with this expression gives

[2.21] $q = (2S \sin a)/L - (8M \cos^2 a)/L^2 + (q \cos^2 a)/4$

The coexisting axial load and moment is assumed to be given by

[2.22] $M = Mp [1 - (S/S_y)^2]$

By replacing the expression for M of [2.22] in [2.21] and
then partially differentiating this new expression with
respect to S and setting the result equal to zero,
equivalent to stating that the load is carried by the
stiffest path, i.e. the membrane force S, the membrane force
is found to be

[2.23] $S = (LS_y^2 \sin a)/8Mp$

Substituting this expression and that for M of [2.22] in
[2.21] gives

[2.24] $q = 16Mp/L^2 + (S_y^2 \sin^2 a)/4Mp$

Furthermore, dividing [2.24] by the critical load of [2.4]
results in the following nondimensional expression relating
load to maximum deflect:

$$[2.25] \quad \frac{q}{q_c} = 1 + \left[\frac{W_{max}}{h} \right]^2 \frac{(1 - \nu_p^2)^2}{(1 - \nu^2)^2} \frac{1}{\left[1 + 4(W_{max}/L)^2 \right]}$$

To obtain [2.25], sin a was replaced by using the following expression:

$$[2.26] \quad \tan a = 2W_{max}/L$$

Expression [2.25] is plotted in Fig. 2.7 as curve Y. It starts with zero deflection at the collapse load as was assumed in the analysis, and becomes tangent to curve M_i derived in Chapter 3 which describes the limiting load for full membrane action when tensile yielding of the cross-section has occured. As curve Y is based on full yielding of the cross-section, first in flexure and then in tension, it must represent an upper-bound to the true behaviour.

2.7 Summary

The uniform transverse flexural collapse load, generally used as a strength criterion in the design of flat plate structures does not reflect the true strength inherent

in continuous plating. As plate deflections increase, membrane forces develop and the overall plate strength increases. Continuous plate that is designed without deflection limits can resist transverse loads many times that predicted by elastic, elasto-plastic and plastic mechanism analyses.

The elastic solution of Timoshenko for the load-deflection behaviour of plates having aspect ratios approaching zero has been validated by tests, even when extended up to complete plastic hinge formation at the plate edges. However, no analytical solution appears adequate to define the behaviour after edge hinge formation and prior to complete yielding of the plate cross-section in tension. Solutions available for the inelastic behaviour of plates having aspect ratios other than zero do not predict well the load-deflection behaviour. Young's limiting curve for inelastic membrane behaviour is in reasonable agreement with his test results. By assuming that plastic hinges due to flexural action have formed a mechanism and that the material behaves elasto-plastically, an upper bound to the true load-deflection behaviour has been established as an extension of the work of Kennedy and Hafez. Strain-hardening effects have generally been neglected by previous authors and no ultimate strength predictions and failure criteria have been established. Furthermore, methods of providing adequate restraint such that the membrane forces can be developed in a flat plate structure have not been discussed.

3. NEW METHOD OF ANALYSIS

3.1 Introduction

In the literature reviewed on the analysis of
continuous rectangular steel plates subjected to transverse
loads, both the contribution to strength by the flexural
action and the membrane action have been considered. Lower
and upper bounds to the true behaviour may, however, be
established simply by neglecting either the bending or
flexural resistance of the plate and considering the other.

3.2 Membrane Analysis Without Strain-Hardening

For a given deflection, a plate acting as a membrane
and with bending resistance is stronger than one without
bending resistance. As a corollary, for a given transverse
load a plate with bending resistance would have less
deflection. Consider a plate of zero aspect ratio, no
flexural resistance, clamped against translation at the
edges and of width L subject to a uniformly distributed load
q. From the free body diagram of a unit width of such a
plate, shown in Fig. 3.1, by statics,

[3.1] $$q = \frac{2Pw}{x(L - x)}$$

The maximum deflection at x equal to L/2 is

29
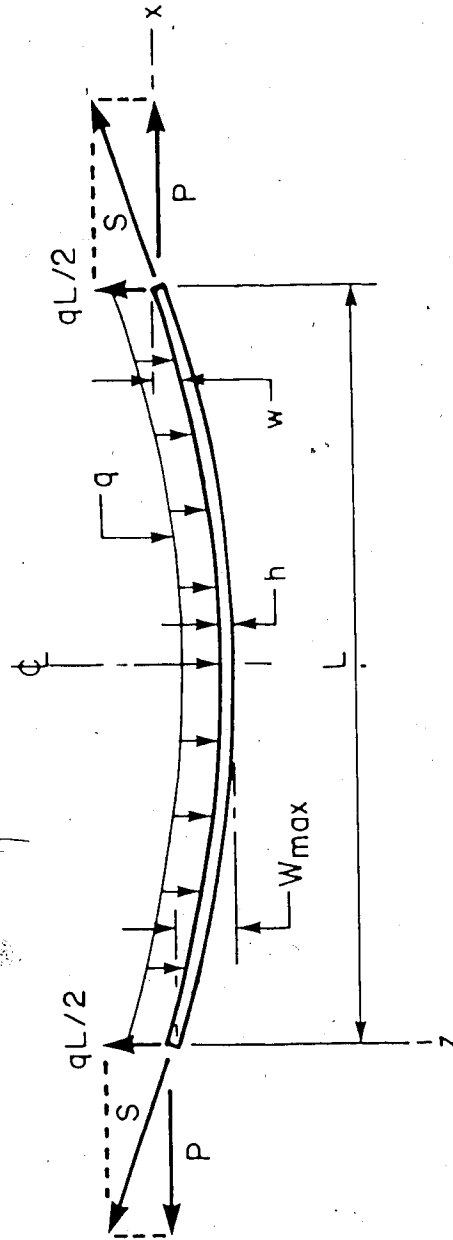
Figure 3.1 Free body diagram of plate acting as a membrane

[3.2] $W_{max} = \dfrac{qL^2}{8P}$

The membrane force S is a maximum at the edge of the plate and is

[3.3] $S = \sqrt{P^2 + \left[\dfrac{qL}{2}\right]^2}$

Combining [3.2] and [3.3] gives

[3.4] $q = \dfrac{8W_{max}S}{\sqrt{L^4 + (4W_{max}L)^2}}$

The slope of the membrane from [3.1] is

[3.5] $\dfrac{dw}{dx} = \dfrac{q}{2P}(L - 2x)$

and using [3.2],

[3.6] $\dfrac{dw}{dx}$ = $\dfrac{4W_{max}}{L^2}$ (L - 2x)

By assuming relatively small deflections, i.e. neglecting the square of differentials, the elongation of the half length of the midsurface of the membrane from [2.12] and [3.6], is

[3.7] λ = $\displaystyle\int_0^{L/2} \dfrac{16W_{max}^2}{L^4} [L^2 - 4xL + 4x^2]\, dx$

and

[3.8] λ = $\dfrac{8W_{max}^2}{3L}$

The closed-form solution of [3.8] is more convenient than that found using the exact expression,

$$[3.9] \qquad \lambda = \int_0^L \left[\left[\left[\frac{dw}{dx} \right]^2 + 1 \right]^{1/2} - 1 \right] dx$$

which can only be evaluated by using a binomial expansion. In fact, [3.7] and [3.8] results when only the first term of a binomial expansion is used to evaluate [3.9]. When W_{max}/L is as much as 0.10, the extension, λ, is 2.3% less by [3.9] than by [3.7]. At this deflection the corresponding, strain is 0.0267, approximately 18 times the yield strain for a steel of yield strength of 300 MPa and beyond the strain-hardening strain of common structural steels used in Canada. Assuming that the deflection of the uniformly transversely loaded membrane results solely from uniform straining and that [3.8] is a valid approximation, the mean value of the strain is

$$[3.10] \qquad \epsilon = \frac{8}{3} \left[\frac{W_{max}}{L} \right]^2$$

When the plate is behaving elastically, the strains are small and the assumption of uniform strain is reasonable as the difference between the minimum axial force in the

membrane at the midspan and the maximum at the edge is likely to be less than part of 1 percent. Recognizing the uniaxial plane strain condition, the corresponding maximum membrane force is

$$[3.11] \quad S = \frac{8}{3} \left[\frac{W_{max}}{L} \right]^2 \frac{Eh}{(1 - \nu^2)}$$

Substituting [3.11] in [3.4], the elastic load-deflection relationship of the transversely loaded membrane is

$$[3.12] \quad q = \frac{64}{3} \left[\frac{W_{max}}{L} \right]^3 \frac{Eh}{(1 - \nu^2)} \frac{1}{\sqrt{(L^2 + 4W_{max})^2}}$$

This equation shows that the load carried varies as the cube of the deflection if the ratio W_{max}/L is small. Nondimensionalizing [3.12] by dividing by q_c gives

$$[3.13] \quad \frac{q}{q_c} = \frac{16 \, W_{max}^3 \, E \, (1 - \nu_p^2)}{3hL^2 \sigma_y (1 - \nu^2) \sqrt{1 + (4W_{max}/L)^2}}$$

Equation [3.13] is plotted in Fig. 3.2 as curve M_e. Below and to the right of this curve, because no plate can be more flexible than a membrane with no flectural resistance, is an inadmissable domain. In [3.13] the value of Poisson's ratio used to determine the load q is the elastic value, ν (taken here to be equal to 0.3), because the membrane is behaving elastically. To determine the collapse load, q_c, because the steel will have yielded significantly in bending, Poisson's ratio is taken as $\nu_p = 0.5$, consistent with the hypothesis, as stated previously, that in plastic straining no volume change occurs.

Equations [3.12] and [3.13] are valid only to the load when the maximum membrane force, S, at the edge reaches the yield force. This maximum value of S is $\sigma_y h / (1-\nu_p^2)$, assuming a state of biaxial stress exists in the membrane and that yielding occurs as predicted by the maximum principal strain theory. The deflection corresponding to full membrane yielding at the edges from [3.11] is

$$[3.14] \qquad (W_{max})_y = L \sqrt{\frac{3\sigma_y}{8E}}$$

$$= L/2 \sqrt{1.5\epsilon_y}$$

Point B on Fig. 3.2 corresponds to the deflection given by [3.14]. With further loading beyond point B, yielding
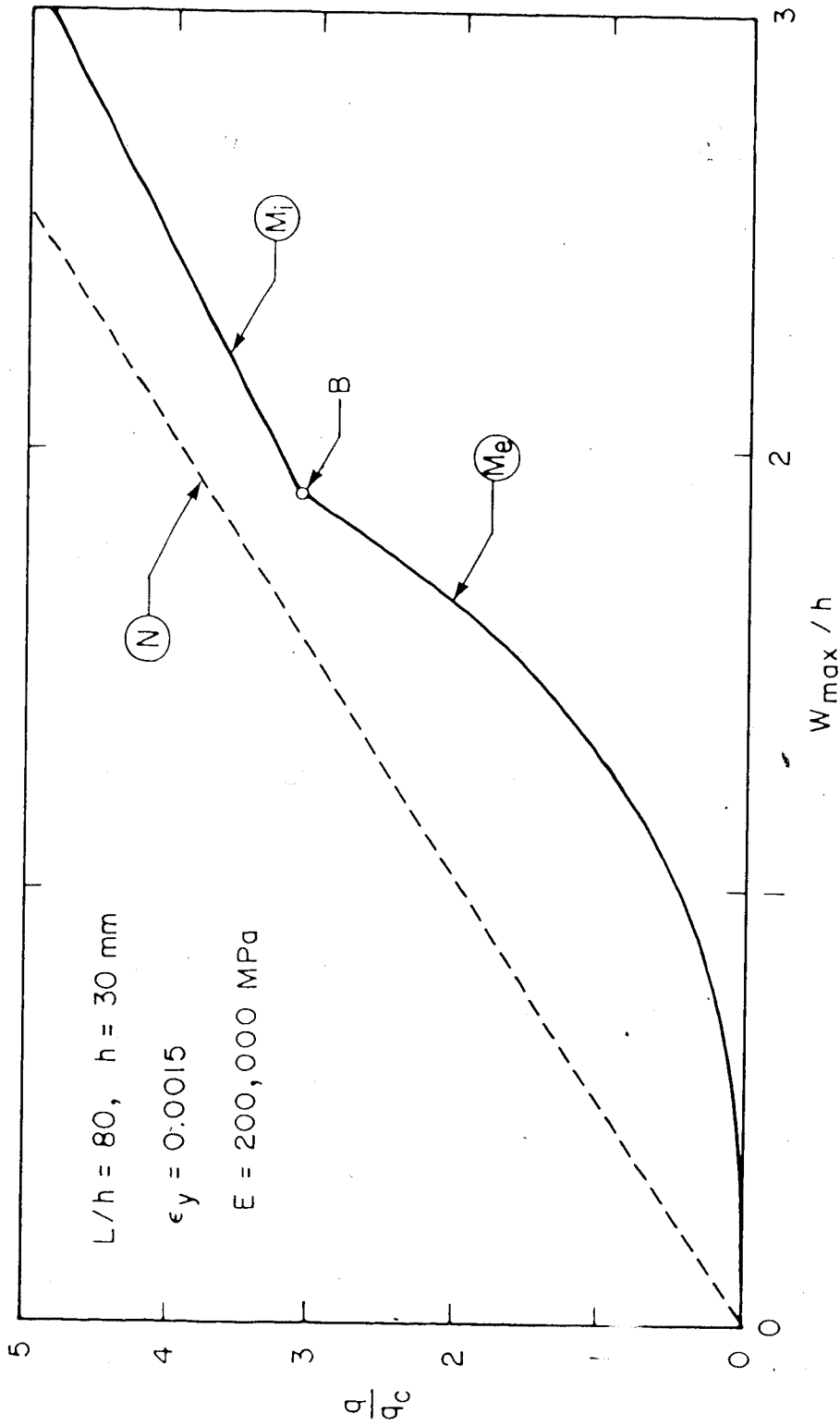
Figure 3.2 Load-deflection behaviour; membrane action only

progresses from the edges towards the centre.

Assuming for the moment that the behaviour is not affected by changes in Poisson's ratio due to yielding, the membrane is capable of carrying an increased load even when the maximum stress at the edge remains at the yield level because of the increased angle of inclination at the edges that results through further deflection. This increased deflection results from the increased straining beyond the yield strain that gradually progresses from the edges towards the centre, until the entire membrane is strained beyond the yield strain and into the strain-hardening region. When the membrane is fully yielded from edge to edge, the membrane force, a maximum at the edge, will exceed the yield force. Notwithstanding this, if it is assumed that the maximum membrane force given by [3.11] is equal to the yield force, and nondimensionalizing [3.4] by the collapse load, q_c, gives

$$[3.15] \qquad \frac{q}{q_c} = 2 \left[\frac{W_{max}}{h} \right] \frac{(1 - \nu_p^2)}{(1 - \nu^2)} \frac{1}{\sqrt{1 + (4W_{max}/L)^2}}$$

Plotted in Fig. 3.2 as curve M_i, [3.15] deviates only slightly from a straight line because of the square-root term containing the ratio W_{max}/L. However, if for any zone that has yielded a Poisson's ratio of 0.5 is used, [3.15]

becomes

$$[3.16] \qquad \frac{q}{q_c} = 2\left[\frac{W_{max}}{h}\right] \frac{1}{\sqrt{1 + (4W_{max}/L)^2}}$$

In Fig. 3.2, [3.16] shown as curve N deviates from Young's linear relationship, [2.16], by the square-root term. Loads given by [3.16] only apply after yielding has progressed to the centre. Therefore, after a membrane is loaded beyond the point at which yielding occurs at the edge (point B of Fig. 3.2) the load-deflection path would be expected to gradually migrate from that given by [3.15] to that given by [3.16]. Now, considering that when the membrane is fully yielded from edge to edge, that the maximum membrane force at the edge will exceed the yield force, the load-deflection path could therefore eventually lie even above curve N when strain-hardening is taken into account.

3.3 Permissible Domain of Behaviour

The analyses presented and those reviewed in the literature form a permissible domain of behaviour, as shown in Fig. 3.3, for a plate of zero aspect ratio and an L/h of 57.1. Curve F gives the load-deflection response assuming that flexural action only occurs. If membrane action occurs in the plate as well, the load-deflection response must lie
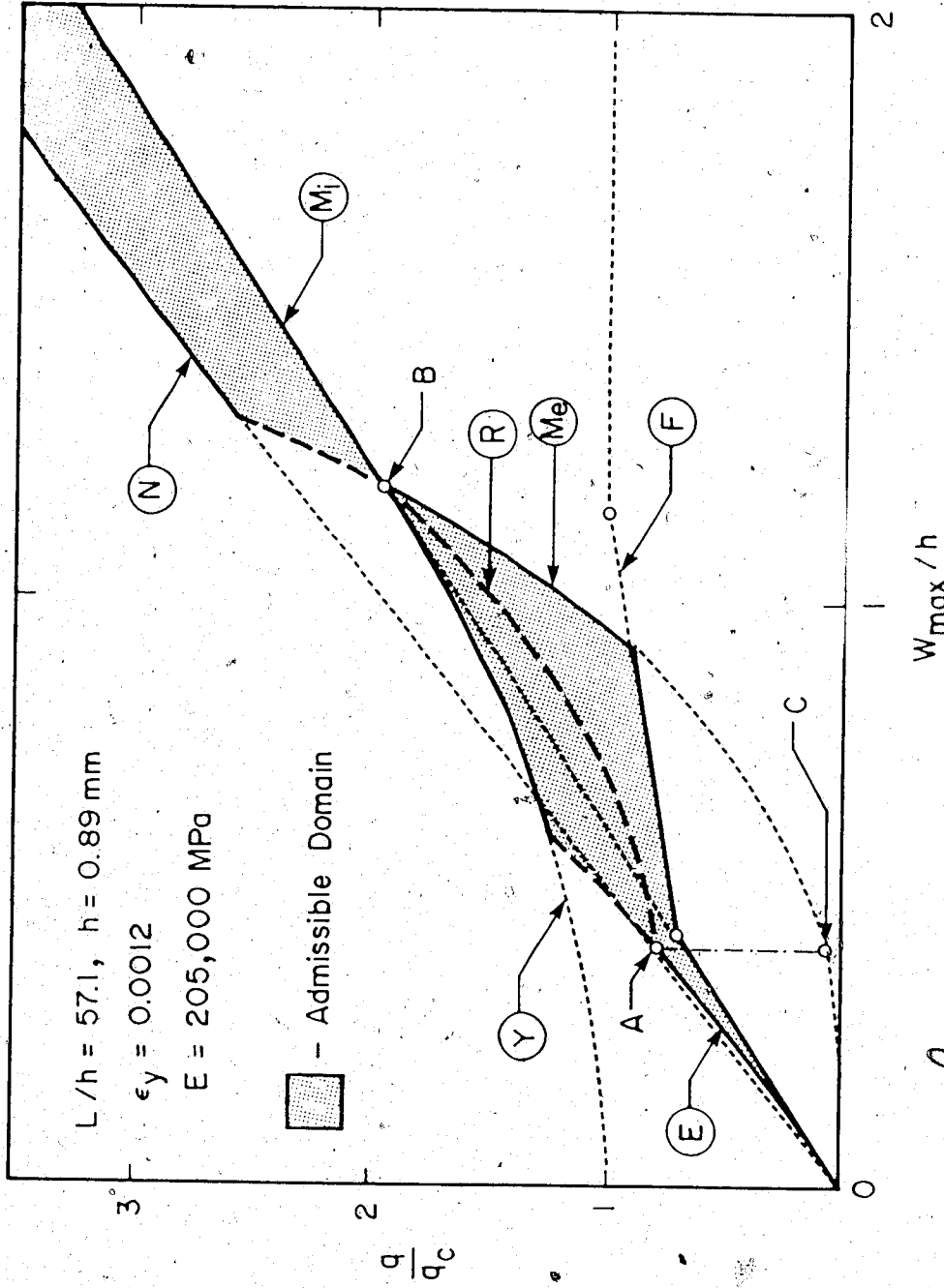
Figure 3.3 Behavioural domain without strain hardening

L/h = 57.1, h = 0.89 mm
$\epsilon_y = 0.0012$
E = 205,000 MPa

– Admissible Domain

above curve F. Curve M_e describes the response when membrane action only exists and the behaviour is elastic. This curve reaches a limiting value at point B when full yielding of the cross-section in tension occurs. Beyond point B, curve M_i, based on a lower limit to Poisson's ratio of 0.3 in the inelastic range and an elasto-plastic stress-strain curve (no strain-hardening), describes inelastic membrane behaviour with deflections increasing as the result of inelastic strains.

The load-deflection response of a real infinitely long continuous plate should not lie below any of these curves. Where one of these curves lies below another it is shown as a dashed line.

Again ignoring strain-hardening, curve N is based on an inelastic Poisson's ratio of 0.5. Hence, to the right of point B, that is for relatively large deflections, the load-deflection response, without considering strain-hardening, should lie in the shaded area between curves N and M_i and beyond curve M_e as extended through point B

The curve presuming full yielding of the cross-section, first in flexure and then in tension, based on Kennedy and Hafez (1984), is shown as curve Y in Fig. 3.3. Apart from considerations of the change in Poisson's ratio or strain-hardening, this curve represents an upper limit to any load-deflection response.

The elastic flexural membrane response derived by Timoshenko (1940) is shown in Fig. 3.3 as curve E extended to point A, as validated by test; based on the assumption that the moment-curvature relationship is elasto-plastic. Curve E is extended as an upper bound, assuming continued flexural and membrane load carrying capacity beyond the yield value, to intersect curve Y. Therefore, to the left of point B the real behaviour of a transversely loaded flat plate would be expected to lie within the shaded area bounded by curves F and M_e providing the lower limit, and by curves E and Y providing the upper limit. When strain-hardening is considered, the real load-deflection curve to the right of point B would be expected to lie eventually above curve N.

3.3.1 Postulated Behaviour Without Strain-Hardening

As derived by Timoshenko and corroborated by test the initial load-deflection response is elastic flexural membrane action as given by curve E, up to point A in Fig.3.3. Beyond this point, increasing tensile straining gradually obliterates the bending stresses until the limiting condition of full tensile yielding of the plate occurs at point B which is the limit of curve M_e describing elastic membrane behaviour.

A curve can easily be constructed between points A and B recognizing that the load-carrying contribution of flexural action gradually disappears between these two

points. Such a curve, assuming that the flexural contribution decreases parabolically, consistent with the interaction relationship between axial force and moment for a rectangular section, is drawn in Fig. 3.3 and labelled curve R. The flexural contribution has been taken to be the difference between the ordinate of point A on curve E and the ordinate of point C on the membrane curve, M_e, directly below it. This simplified analysis contains two counteracting assumptions:

(i) A parabolic decrement applied over the entire range from A to B is strictly only true if the axial load at point A were zero. Such is not the case and therefore the curve from A to B, based on this assumption, would tend to be too high.

(ii) While the moment developed at the edge is decreasing there is an increasing moment at midspan. Therefore, the curve would be too low. This assumption counteracts that given above.

To the left of point B flexural and membrane action coexist. To the right of point B, there is no flexural action and the load-deflection response would be expected to gradually move from curve M_i towards curve N as yielding progresses from the edges towards the centre and more and more of the membrane has an inelastic Poisson's ratio.

3.3.2 Significance of Strain-Hardening

'Strain-hardening comes into play in two different ways.
When plastic hinges rotate through significant angles,
strain-hardening is likely to occur in the extreme fibres.
Galambos et al. (1978) show that the mean test to predicted
ratio of the fully plastic moment for W shapes is 1.12. This
increase of 12% is probably chiefly due to strain-hardening.
For plates of rectangular cross-section the effect would be
expected to be less. The most important effect of strains
greater than strain-hardening is the increased tensile
capacity of the plate associated with such strains coupled
with the increased deflections that result, thus providing
more efficient membrane action. Therefore, to the right of
point B the real load-deflection curve would be expected to
lie eventually above curve N based on an elasto-plastic
stress-strain curve. Provided local effects do not dominate,
the steel is finally strained to the ultimate, at least in
some portions of the membrane.

3.4 Membrane Analysis Beyond Strain-Hardening

The load-deflection response of a plate of zero aspect
ratio subject to fluid pressure, as opposed to a uniform
transverse load, can easily be determined when the plate
acts purely as a membrane. For a given pressure, the
membrane force is constant across the short dimension, L.
Corresponding values of the membrane stress and strain are
obtained from the stress-strain curve of the plate material.

The strain determines the total extended length of the membrane and the deflected shape is circular. Because the strain in the long dimension is zero, biaxial tension exists and the effective stress in the membrane is increased by $1/(1-\nu^2)$ times.

Stang et al. (1946) derive, corroborated by experimental evidence, that Poisson's ratio in the inelastic range or beyond initial yielding is

$$[3.17] \qquad \nu_p = \frac{1 - \sqrt{\dfrac{1 + \delta}{1 + \epsilon}}}{\epsilon}$$

where δ is equal to the volume change occuring prior to yielding and ϵ the engineering strain beyond yielding. Equation [3.17] is plotted in Fig. 3.4 for the linearized uniaxial stress-strain curve of Fig. 3.5 and assuming an elastic Poisson's ratio of 0.3 to calculate δ.

Curve U of Fig. 3.6 gives the nondimensional load-deflection curve for a plate of zero aspect ratio subjected to fluid pressure and having the uniaxial stress-strain characteristics given in Fig. 3.5. The kink in the curve at W_{max}/h of about 8.2 marks the onset of strain-hardening of the material. Between point B and the onset of strain-hardening, curve U gradually climbs above curve M_i as a result of the gradually increasing value of Poisson's ratio as given by [3.17]. Also shown on Fig. 3.6
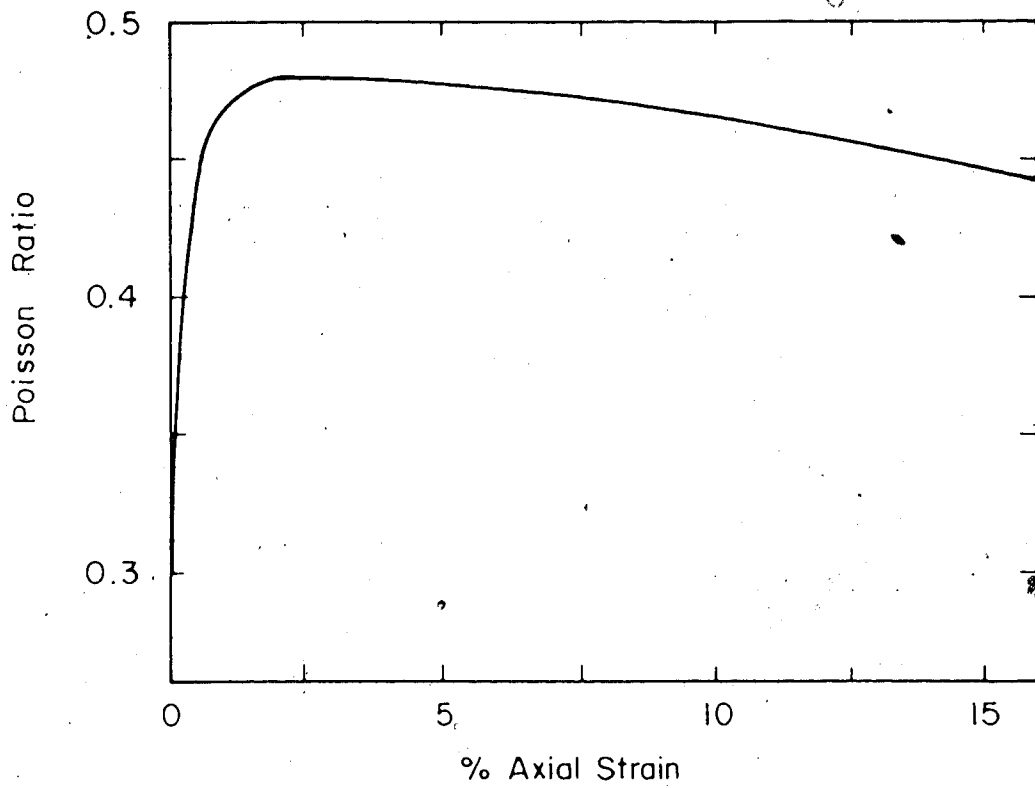
Figure 3.4 Variation of Poisson's ratio with axial strain
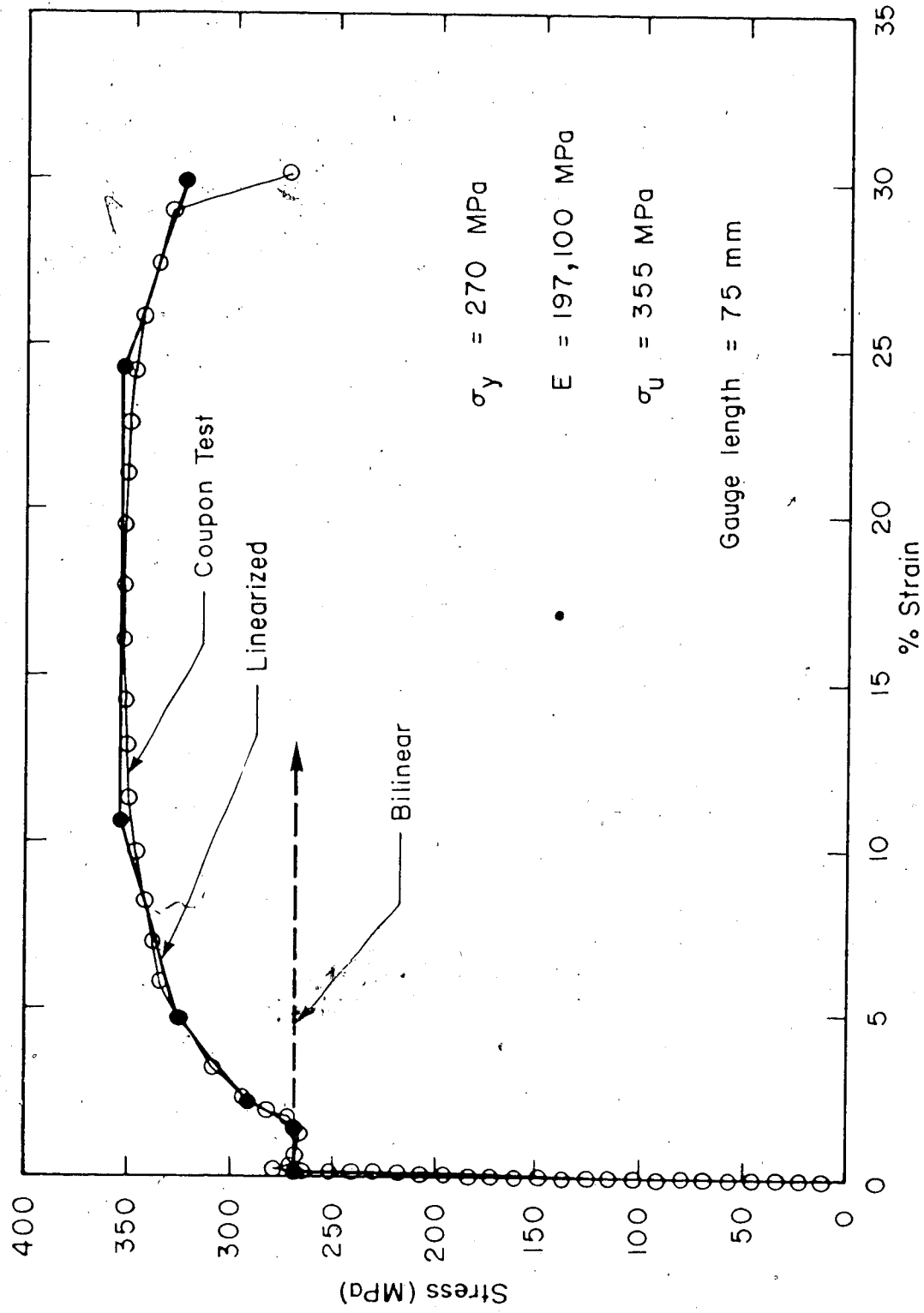
Figure 3.5 Uniaxial tension test results with linearized approximations
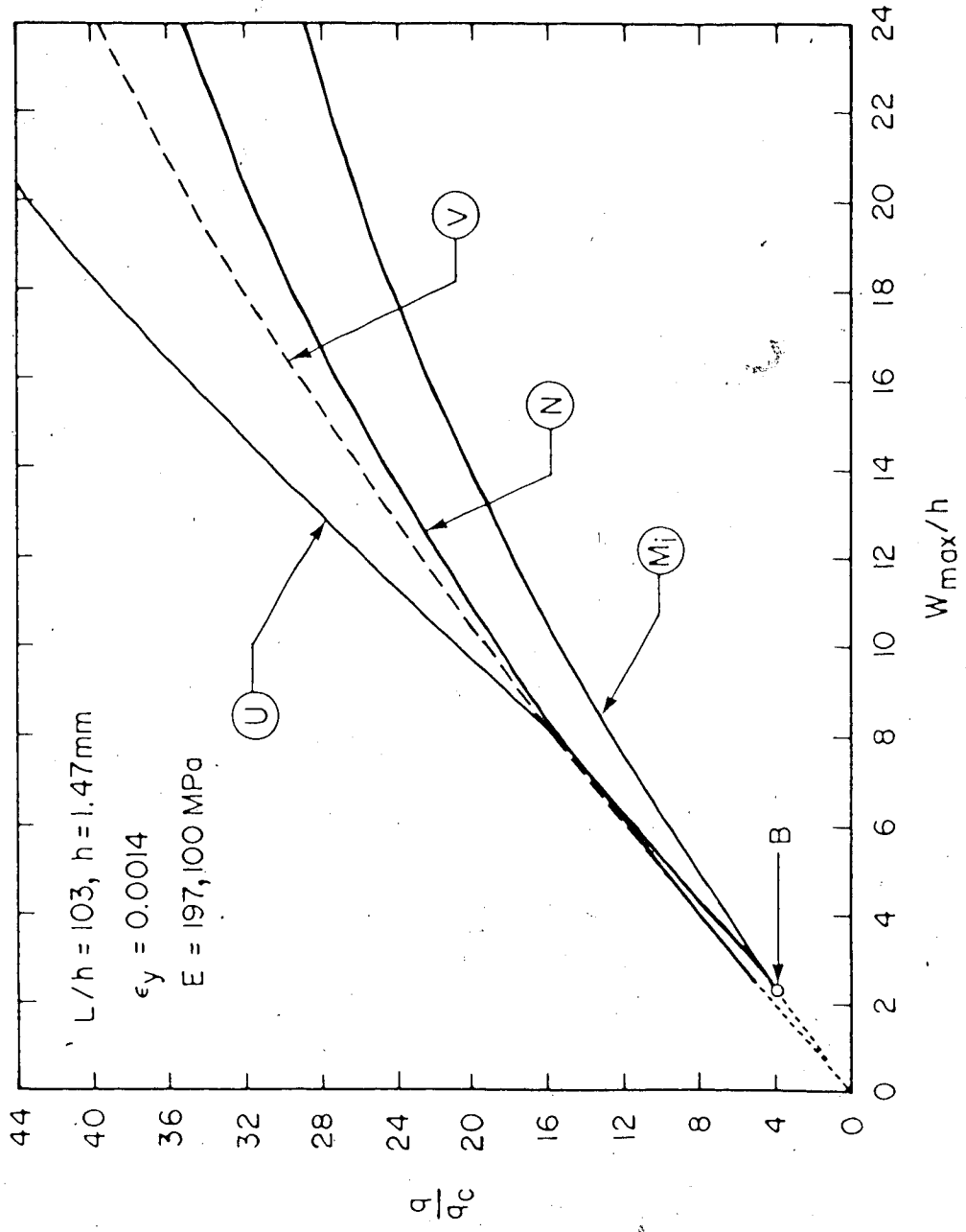
Figure 3.6 Load-deflection behaviour of inelastic membrane

is curve V that is derived based on the same assumptions as used for curve U but with the maximum stress set equal to the yield stress. The difference between curves U and V is therefore attributable to the increase in strength of the material following strain-hardening.

The difference between curves V and N, both based on a maximum uniaxial tensile stress of σ_y, is attributable to the difference in loading. Curve N is for a uniform transverse load and curve V is drawn for a membrane loaded by fluid pressure. Without other effects it would be expected that curve U would extend upward until the ultimate strength of the material in biaxial tension was reached.

3.5 Experimental Verification

Plotted in Fig. 3.7 are test results of Young (1959) for a plate having an aspect ratio of 1/3 and an L/h of 57.1. These data are in reasonable agreement with curves E and R for a zero aspect ratio. Hooke (1970) showed that it was valid to compare the maximum deflection determined experimentally for plates with an aspect ratio of less than 1/2 to the analytical value for plates of zero aspect ratio. Above and to the right of point B, the experimental results gradually move from curve M_i to N and as proposed previously and even slightly exceed it.

In Fig. 3.8 similar curves, for a plate with an L/h of 49.4, are compared with the test results of Young, again for a plate with an aspect ratio of 1/3. The test results are in
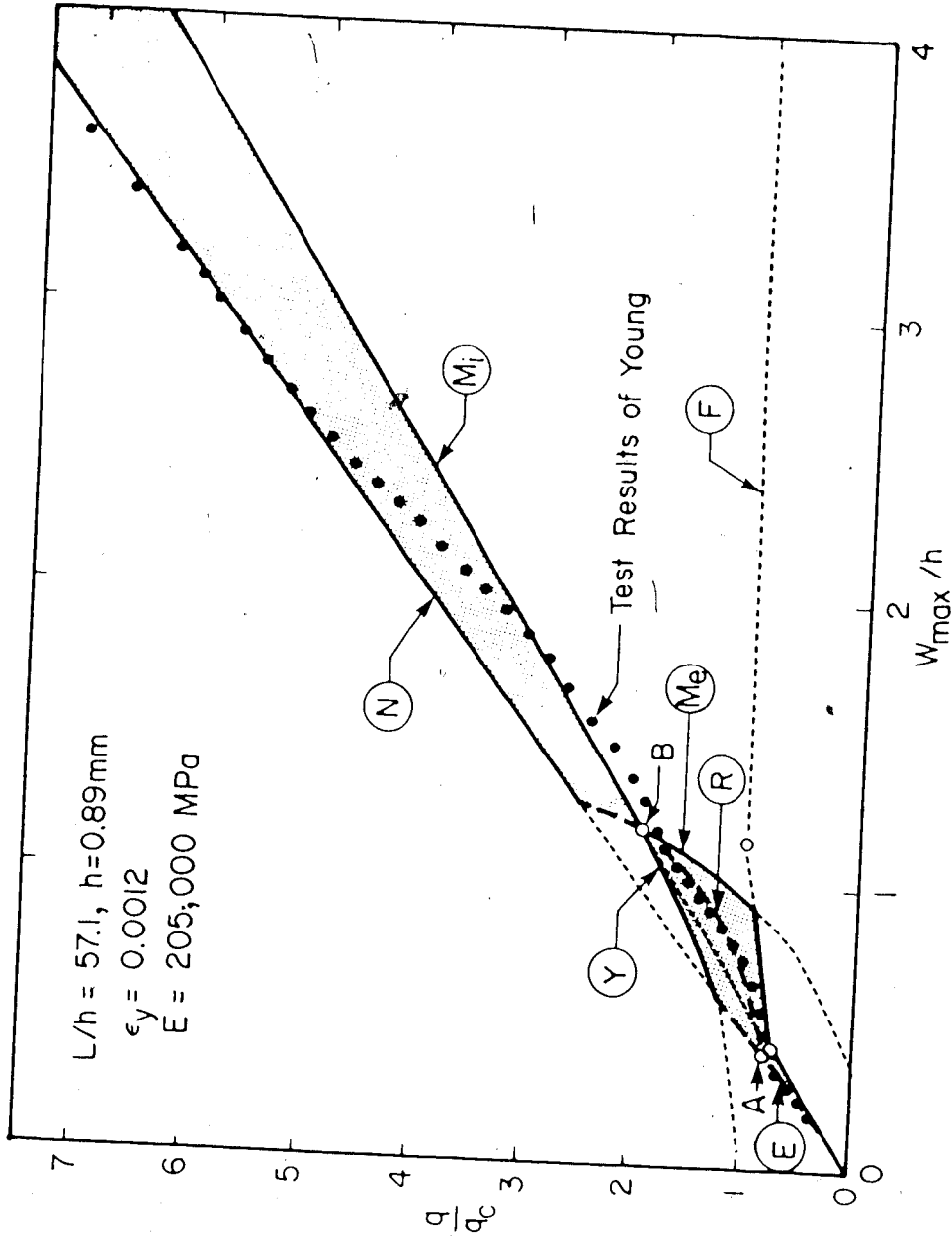
Figure 3.7 Test results of Young(1959) and behavioural domain
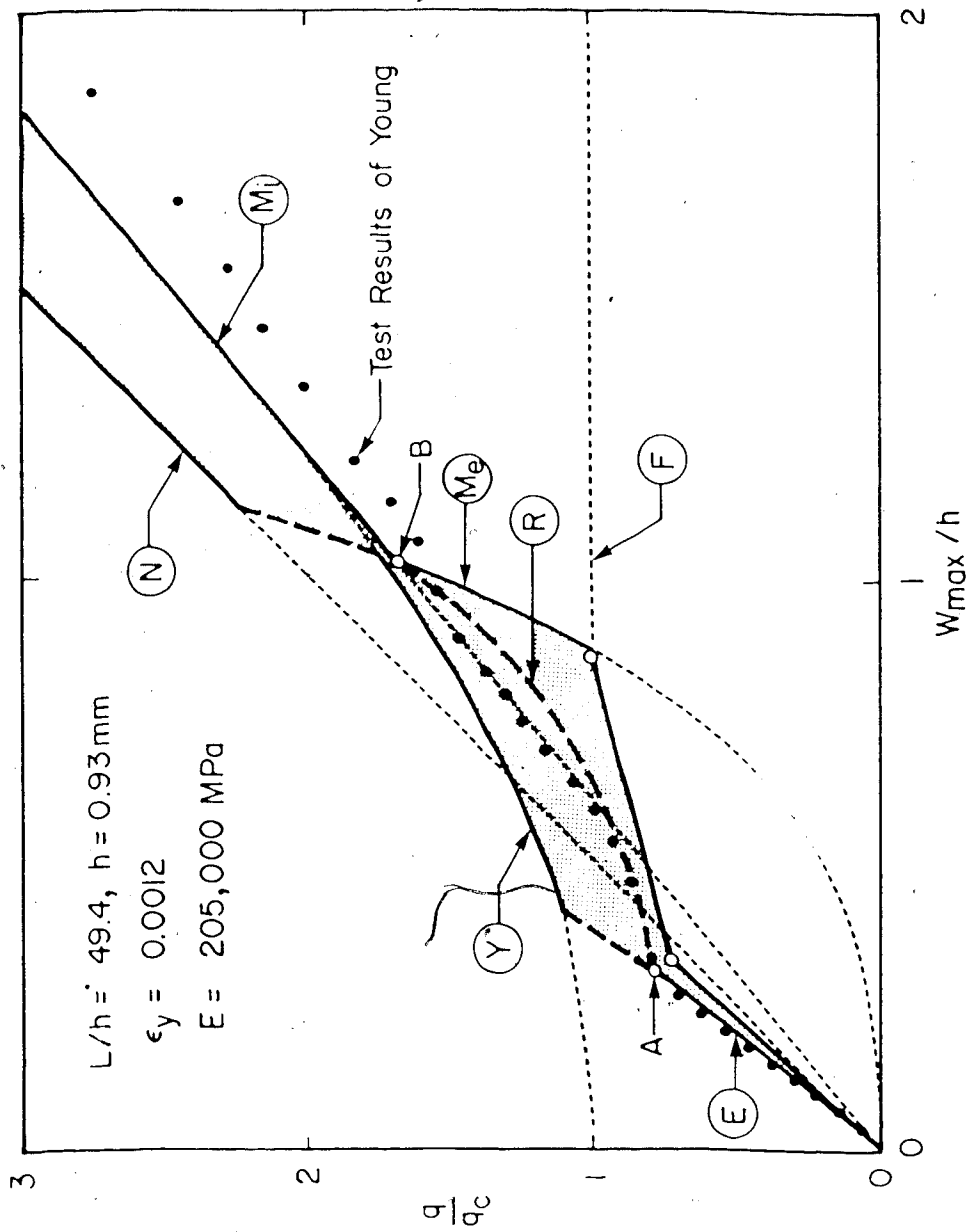
Figure 3.8 Test results of Young(1959) and behavioural domain

reasonable agreement with the postulated behaviour, although
falling below curve M_i. It is possible that inward movement
of the edges of the plate resulted in increased deflections
at the higher load levels. Although the experimental results
tend to follow a portion of the extension of curve M_i to the
left of point B, and above curve R, this must be considered
a coincidence as curve M_i is not valid to the left of point
B where flexural action contributes to the plate strength.

4. EDGE EFFECTS AND ULTIMATE STRENGTH ANALYSES

4.1 Introduction

All the relationships describing pure membrane action (curves M_i, N, U, and V of Fig. 3.6) are based on the common assumption of considering the plate to have zero thickness. However, to accomodate the relatively large deformations the plate of finite thickness must bend at the edges to achieve the membrane edge slope required. Significant transverse shears also exist at the edges even though no transverse shears exist when the plate acts solely as a membrane. These effects may limit the load that can be carried by the plate.

The deformations that the plate undergoes are also affected by the edge conditions. Away from the edges the membrane is relatively stiff. At the edges the plate is subjected to both flexural and shear stresses in addition to membrane stresses. Though this zone is of limited extent, its flexural and shearing deformations may have a not insignificant effect on the total deflection of the plate.

4.2 Local Bending

4.2.1 Uniform Transverse Loading

Fig. 4.1 illustrates the edge conditions of a plate of span L. When the deflection of the membrane is relatively small as shown in Case I the eccentricity of the membrane force S about the intersection of the edge and the

52
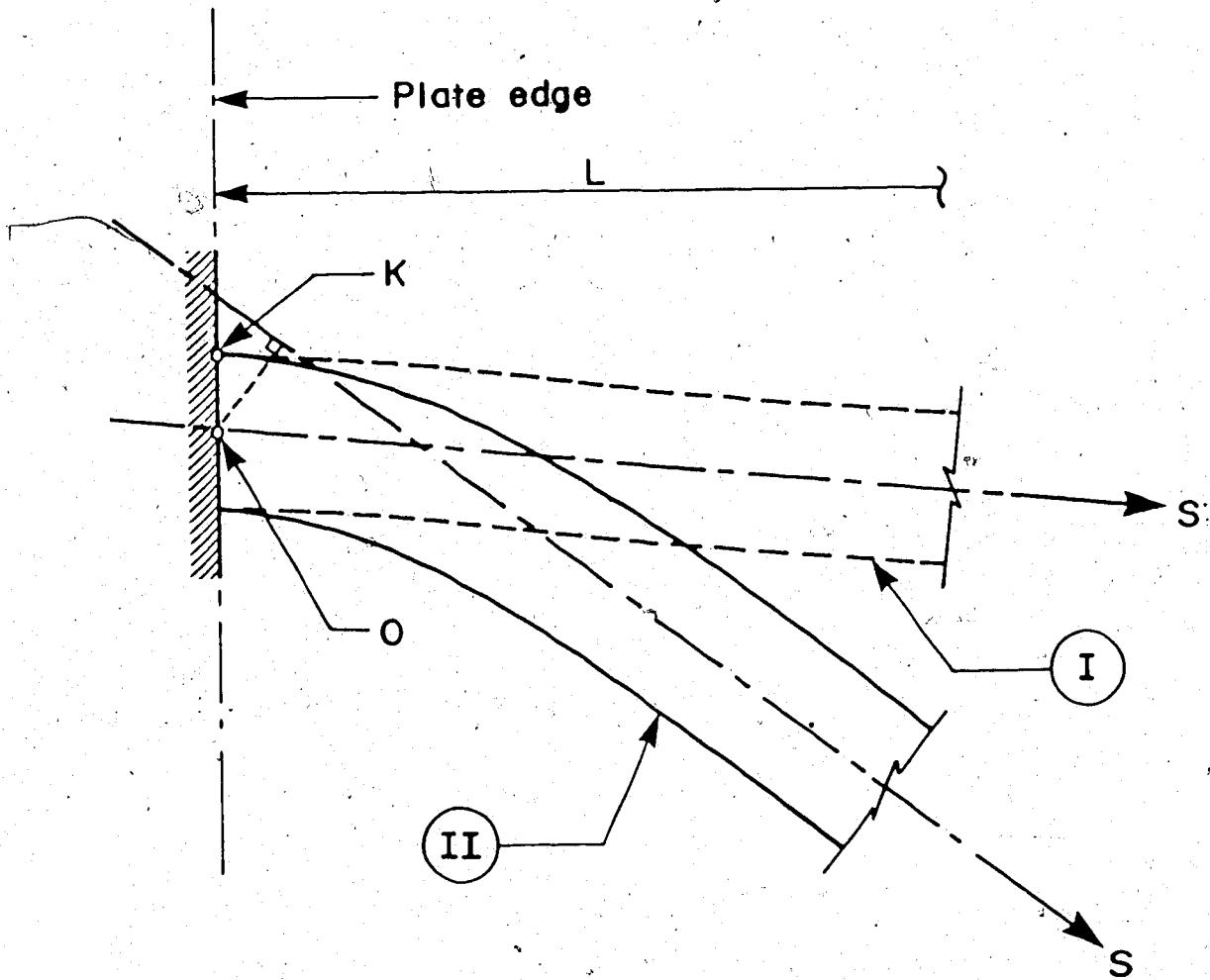
Figure 4.1 Membrane edge conditions

midsurface, point O, is also relatively small. With further loading more extensive bending is required at the edge and a larger eccentricity of the force results as shown in case II. Thus, with increased deflections even though the plate is acting essentially as a membrane, the moment at the edge is re-established. This local bending phenomenon is non-trivial when the curvature strains are large. The largest strains exist at the edge of the plate on the loaded face, point K, where tensile strains due to bending and membrane action are additive. A proposed failure criterion is that failure or rupture occurs when the strain at point K reaches the ultimate strain, ϵ_u, in biaxial tension.

Assuming that the strain distribution at the cross-section through points O and K is linear with an average axial strain, ϵ_p, equal to that due to the axial force Po (see Fig. 4.2), when the maximum strain due to bending and axial forces equals ϵ_u at point K, the radius of curvature is

[4.1] $$\rho_c = \frac{h(1 + \epsilon_p)}{2(\epsilon_u - \epsilon_p)}$$

Considering the free body diagram of a unit width of plate at its edge shown in Fig. 4.2, at point A, a small distance from the edge, the bending moment is zero. Therefore, beyond A, towards the centre, only membrane
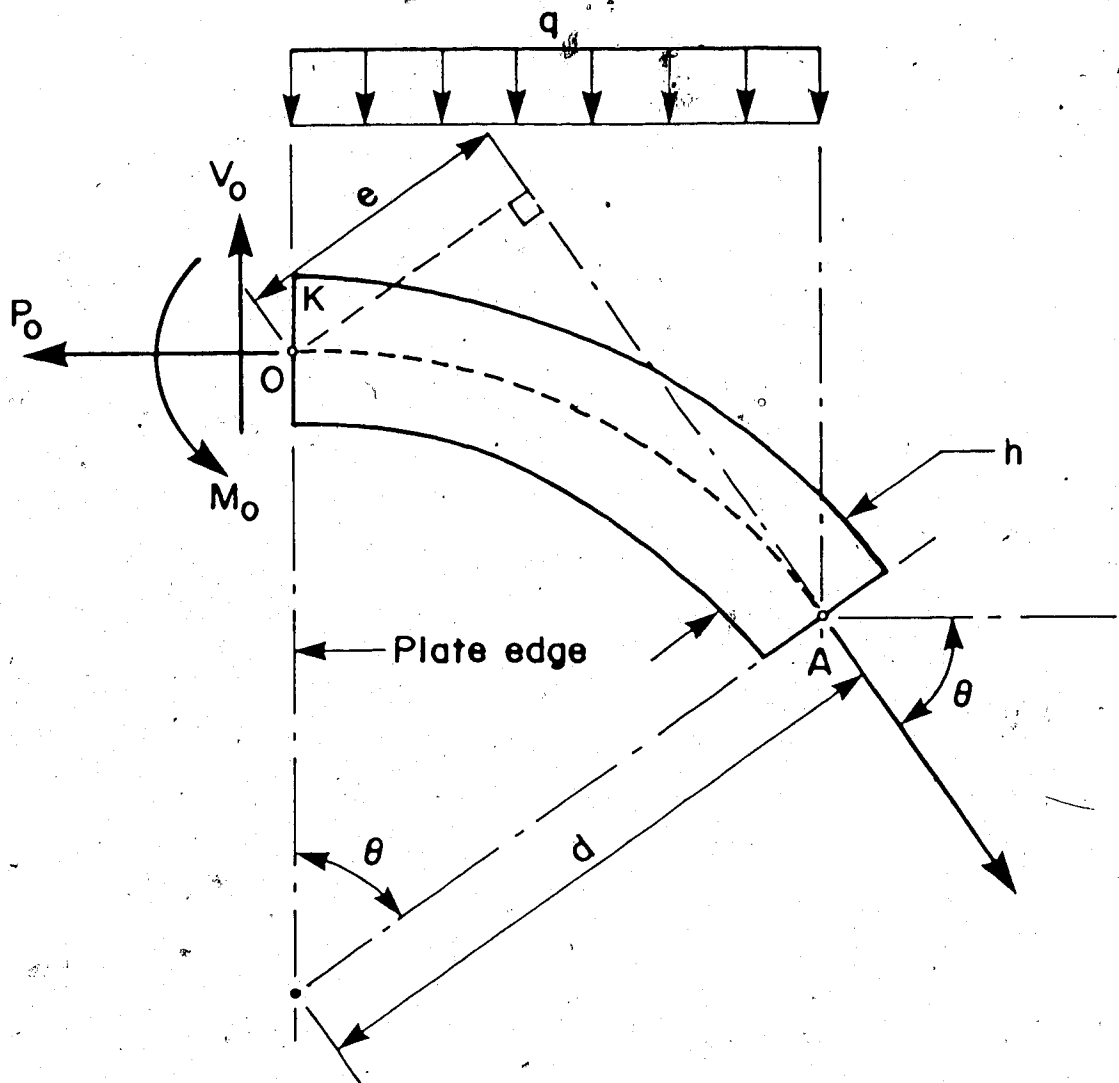
Figure 4.2 Free body diagram of plate at edge

action occurs. The angle of the membrane, θ, at A is the membrane edge inclination or more simply the edge inclination. Assuming that the centreline of the deformed plate shape between O and A can be described by a cubic -function, the minimum radius of curvature corresponding to the maximum bending strains at the plate edge is by geometry,

$$[4.2] \qquad \rho_{min} = \frac{d \cos \theta}{2}$$

McDermott et al. (1974) also used a cubic function to describe the geometry with curvature ranging from zero at point A to a maximum value at the plate edge, when analyzing hull damage from ship collisions.

From geometry, the eccentricity, e, of the maximum membrane force, S, is

$$[4.3] \qquad e = \frac{d \sin^2 \theta}{3}$$

Summing moments about point O and considering centreline dimensions, the moment at the edge is

$$[4.4] \quad Mo = Se + \frac{q\ d^2\ \sin^2\ \theta}{2}$$

The axial force, Po, is

$$[4.5] \quad Po = S \cos \theta$$

Setting ρ_{min} of [4.2] equal to ρ_c of [4.1], gives

$$[4.6] \quad d = \frac{h(1 + \epsilon_p)}{\cos \theta\ (\epsilon_u - \epsilon_p)}$$

Substituting [4.6] in [4.3] gives

$$[4.7] \quad e = \frac{h \sin^2 \theta\ (1 + \epsilon_p)}{3 \cos \theta\ (\epsilon_u - \epsilon_p)}$$

Further substitution of [4.6] and [4.7] in [4.4], gives

$$[4.8] \quad Mo = \frac{Sh \sin \theta \ (1+\epsilon_p)}{3 \cos \theta \ (\epsilon_u - \epsilon_p)} + \frac{qh^2 \tan^2\theta \ (1+\epsilon_p)^2}{2(\epsilon_u - \epsilon_p)^2}$$

Under uniaxial plane strain conditions for a unit width of plate, the maximum membrane force corresponding to uniaxial stress-strain condition (σ_s, ϵ_s), based on the maximum principal strain theory, is

$$[4.9] \quad S = \frac{\sigma_s h}{(1 - \nu_s^2)}$$

Substituting [4.9] in [4.8] gives

$$[4.10] \quad Mo = \frac{\sigma_s h^2 \sin^2 \theta \ (1+\epsilon_p)}{3 \cos \theta \ (1 - \nu_s^2)(\epsilon_u - \epsilon_p)}$$
$$+ \frac{qh^2 \tan^2 \theta \ (1+\epsilon_p)^2}{2 \ (\epsilon_u - \epsilon_p)^2}$$

and the same substitution in [4.5]gives

[4.11] $Po = \dfrac{\sigma_s h \cos \theta}{(1 - \nu_s)^2}$

The coexisting axial load and moment under ultimate conditions at the edge as given by the interaction equation for rectangular sections are

[4.12] $\dfrac{Mo}{Mu} + \left[\dfrac{Po}{Pu} \right]^2 = 1$

Because the strains are exceptionally large, Mu is taken as $\sigma_u h^2/4(1-\nu_p^2)$ and Pu is taken as $\sigma_u h/(1-\nu_p^2)$. Substituting Mo and Po of [4.10] and [4.11] respectively in [4.12] gives

[4.13] $\left[\dfrac{\sigma_s}{\sigma_u} \right] \left[\dfrac{4 \sin^2 \theta \,(1+\epsilon_p)(1-\nu_p^2)}{3 \cos \theta \,(\epsilon_u-\epsilon_p)(1-\nu_s^2)} \right]$

$+ \dfrac{2q \tan^2 \theta \,(1-\nu_p^2)(1+\epsilon_p)^2}{\sigma_u \,(\epsilon_u-\epsilon_p)^2}$

$+ \left[\dfrac{\sigma_s}{\sigma_u} \right]^2 \dfrac{(1-\nu_p^2)^2}{(1-\nu_s^2)^2} \cos^2 \theta = 1$

This equation is based on the material properties of the plate $\sigma_s, \sigma_u, \epsilon_u, \epsilon_p, \nu_s$ and ν_p.

Two further equations relating the membrane stress, lateral load and edge inclination are found by considering the equilibrium conditions of the central portion of the deformed plate acting as a membrane and extending from point A, as identified in Fig. 4.2 to the similarly located point A', on the opposite side as shown in Fig. 4.3. The deflected shape of the membrane is parabolic. Using [3.6] with [3.10] gives

$$[4.14] \qquad \tan \theta = (6 \, \epsilon_s)^{1/2}$$

and from [3.4]

$$[4.15] \qquad q = \frac{2 \, \sigma_s h \sin \theta}{(L - 2d \sin \theta)(1 - \nu_s^2)}$$

Equations [4.13], [4.14], and [4.15] are solved iteratively as follows:

(i) For an assumed value of ϵ_s find σ_s from the stress-strain curve of the plate material.

(ii) Compute the edge inclination θ and the lateral load q from [4.14] and [4.15].
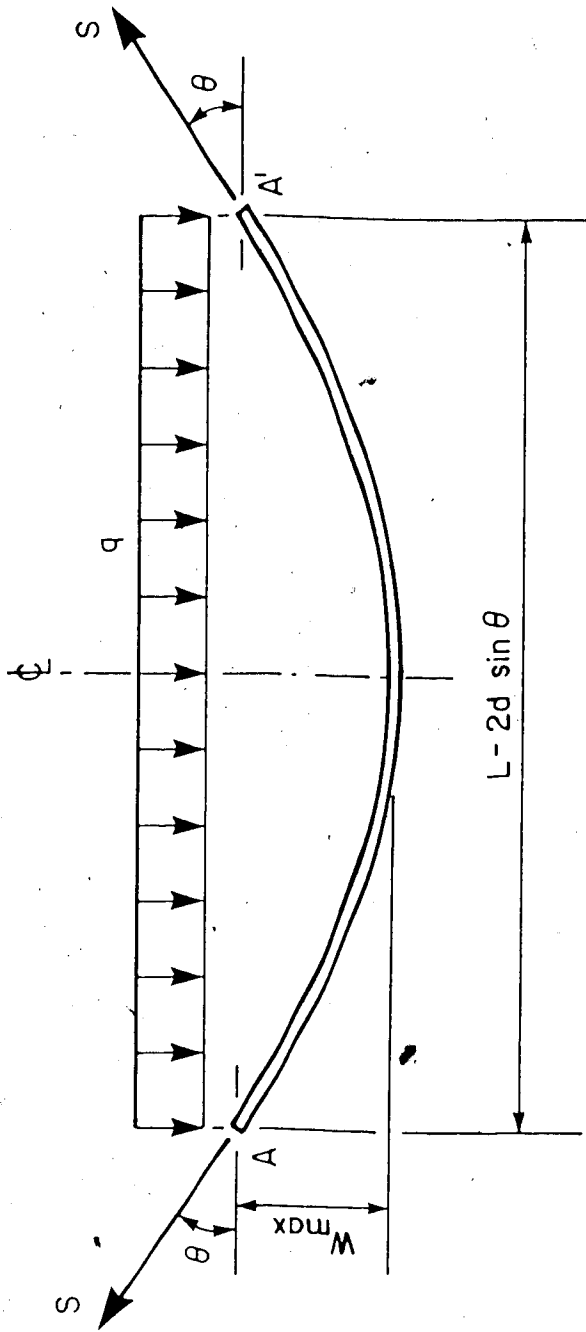
Figure 4.3 Free body diagram of membrane under uniform transverse load

(iii) Substitute the values of ϵ_s, q and θ and relevant material properties in [4.13] and iterate using a new value of ϵ_s until [4.13] is satisfied. The maximum deflection of the membrane is found by rearranging [3.10] and is

[4.16] $W_{max} = (L - 2d \sin \theta)(3\epsilon_s/8)^{1/2}$

Thus, the maximum uniform transverse load and corresponding deflection as limited by local bending at the edges is obtained.

4.2.2 Fluid Pressure Loading

Fig. 4.4 shows a free body diagram of one-half of a membrane strip extending from point A, as identified in Fig. 4.2, to the centreline when the membrane is loaded by fluid pressure. The deflected shape is circular and the following two relationships can be derived:

[4.17] $\dfrac{\sin \theta}{\theta} = \dfrac{\pi}{180 \, (1 + \epsilon_s)}$

[4.18] $W_{max} = (L/2 - d \sin \theta) \dfrac{(1 - \cos \theta)^{1/2}}{(1 + \cos \theta)^{1/2}}$
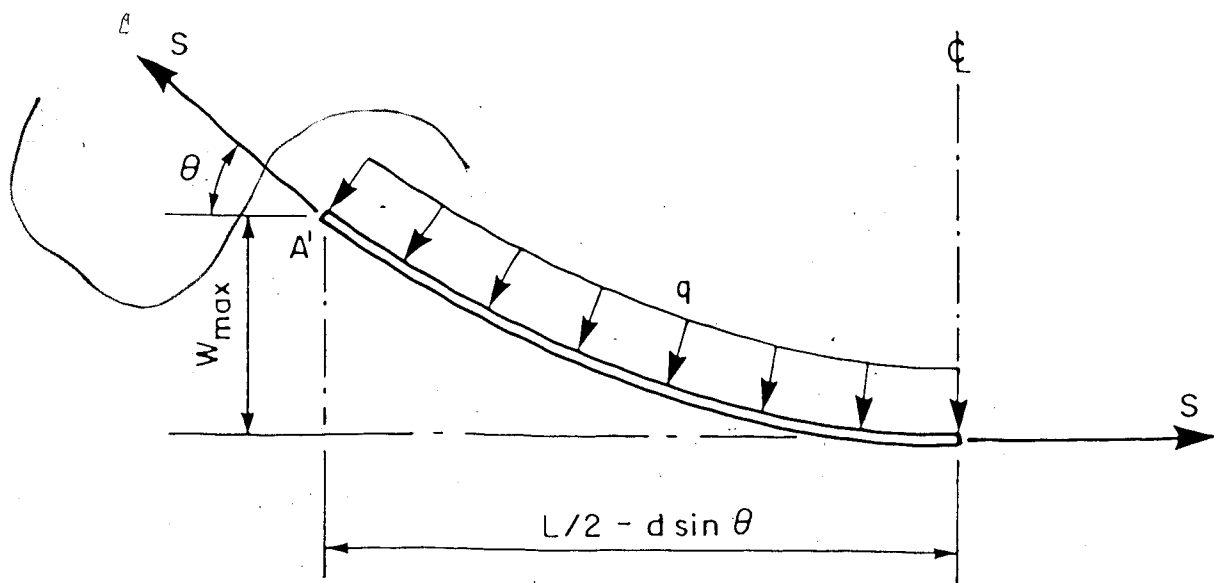
Figure 4.4 Free body diagram of membrane under fluid pressure

where θ is expressed in degrees. Neglecting the weight of the fluid under pressure, a reasonable assumption when the pressure becomes large, the pressure per unit width is equivalent to that given by [4.15]. When considering a membrane subject to fluid pressure, the free body diagram of Fig. 4.2 should be modified to include a lateral load due to this pressure acting over the vertical distance from point O to point A and, as well, the weight of the fluid within these limits. The moments of these forces are relatively small and can be neglected. Again, equations [4.13], [4.15] and [4.17] can be solved iteratively. With the maximum deflection determined from [4.18], the maximum fluid pressure as limited by local bending at the edges is obtained.

4.2.3 Special Considerations

For both loading cases of uniform transverse load and fluid pressure the distance from the edge to point A of Fig. 4.2, where only membrane stresses exist, $d \sin \theta$, is typically only about 2% of the span, L, of the plate.

In [4.13] and [4.15] careful attention must be paid to the values used for Poisson's ratio in the inelastic range and to the maximum strain that can be sustained at the edge. Fig. 3.4 shows that for the strains in the likely range of 3 to 8%, Poisson's ratio varies only between 0.47 and 0.48 for a steel having the stress-strain characteristics shown in Fig. 3.5.

Where maximum straining occurs at the edge the strain gradient is extremely high and therefore the maximum attainable strain should be based on a gauge length approaching zero. Determination of this strain and the corresponding value of Poisson's ratio are given in the section on ancillary tests in Chapter 6.

4.3 Shear Failure

The maximum transverse load that can be carried may be limited by the shear capacity of the plate. For both uniform transverse or fluid pressure loading (neglecting the weight of the fluid), the shear per unit width at the edges of a plate having an aspect ratio approaching zero, is equal to qL/2. Setting this equal to the ultimate shear capacity $\tau_u h$ gives

$$[4.19] \qquad q = \frac{2\,\tau_u h}{L}$$

Metal forming operations show, when a plate is fully restrained in bending and tension at the edges and subject to a sufficiently large hydraulic pressure, that it will shear at the edges similar to the shearing of a high-strength pre-tensioned bolt in a lap joint. CSA Standard CAN3 S16.1-M84, Steel Structures for Buildings – Limit State Design (CSA, 1984) gives the ultimate shear

resistance of such a high-strength bolt as 0.60 $A_b Fu$, as determined experimentally. Based on this evidence it would appear reasonable, as an extension of the von Mises-Huber-Hencky yield criterion to ultimate strength conditions, to take the ultimate strength τ_u in these circumstances as $\sigma_u/\sqrt{3}$ or 0.577 σ_u.

5. FINITE ELEMENT ANALYSES

5.1 Program and Model

The ADINA finite element program (ADINA, 1981) which allows for geometric and material nonlinearities, was used to predict the behaviour of transversely loaded plates of zero aspect ratio.

Fig. 5.1 shows the two-dimensional through-thickness mesh used with 116 elements and 449 nodes for the half width of the plate. All edge elements were linked to the support as all boundary nodes were fixed against translation and rotation. The model therefore did not allow through-thickness straining to occur at the edge.

The plates modelled had an L/h of either 80 or 103 and also had different material properties. The von Mises-Hencky yield criterion for a condition of plane strain was used. Strains were determined at the 2x2 Gaussian integration points of the quadratic serendipity elements. The maximum deflection at the midspan, W_{max}, was taken as the deflection of the midheight node. The uniformly distributed load was applied in increments of 0.1 or 0.2 times the collapse load, q_c, with the smaller load increments applied in regions of inelastic behaviour.
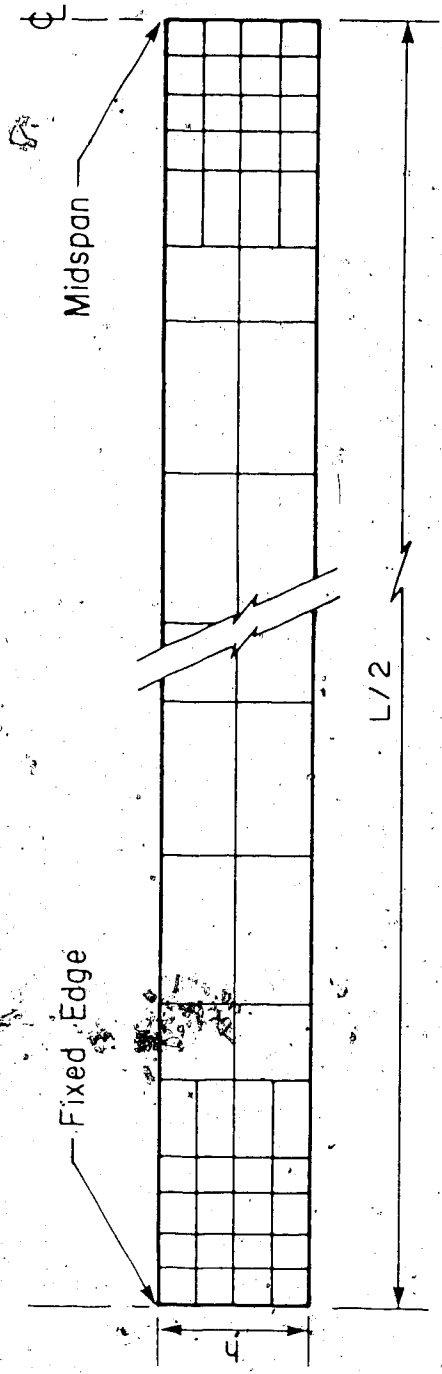
Figure 5.1 Finite element mesh

5.2 Elasto-plastic Analysis

An elasto-plastic finite element analysis was first carried out assuming that the steel had a bilinear uniaxial stress-strain curve although the ADINA program has the capability of modelling a more complex curve. Two elasto-plastic material models were considered. The first, used for the plate model with an L/h ratio equal to 80 was assumed to have a modulus of elasticity of 200,000 MPa and a yield strain of 0.0015. The second, used for the model with L/h equal to 103 and with a stress-strain curve as shown in Fig. 3.5 where is also given the experimental results, was assumed to have a modulus of elasticity of 197,100 MPa and a yield strain of 0.0014. In both cases, Poisson's ratio was taken to be 0.3 in the elastic range and 0.5 in the inelastic range.

The resulting nondimensional load-deflection curves for the two plates are shown in Fig. 5.2 and Fig. 5.3 respectively along with load-deflection curves derived analytically. Curve N models inelastic membrane behaviour with the maximum stress equal to the yield stress and an effective Poisson's ratio of 0.5.

The elasto-plastic finite element results are in reasonable agreement with the postulated behaviour but two differences are evident. First, the slope of the load-deflection curve decreases when deflections exceed about 3h and the finite element results for large deflections fall below both curves N and Mi. This is
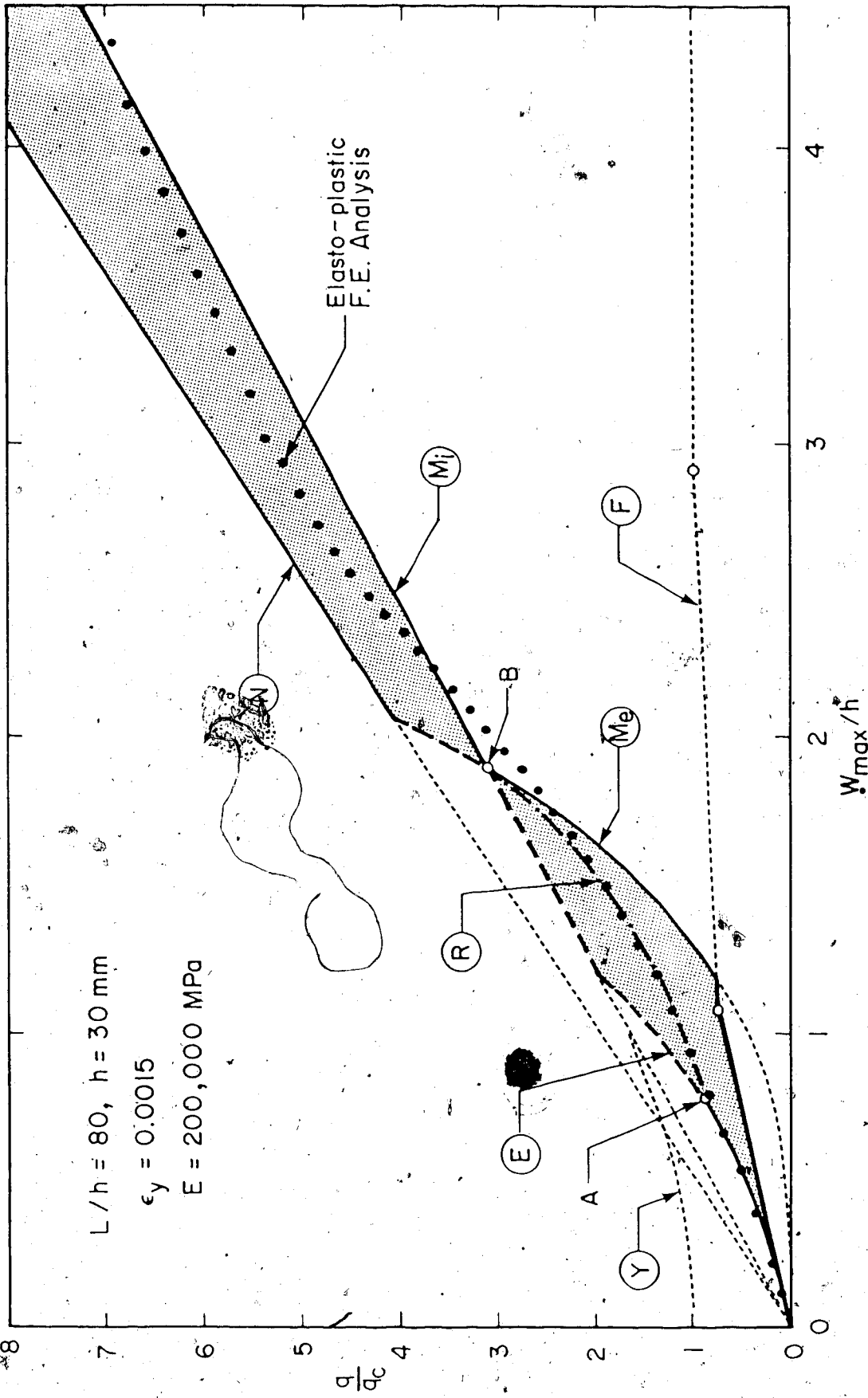
Figure 5.2 Elasto-plastic finite element results and behavioural domain
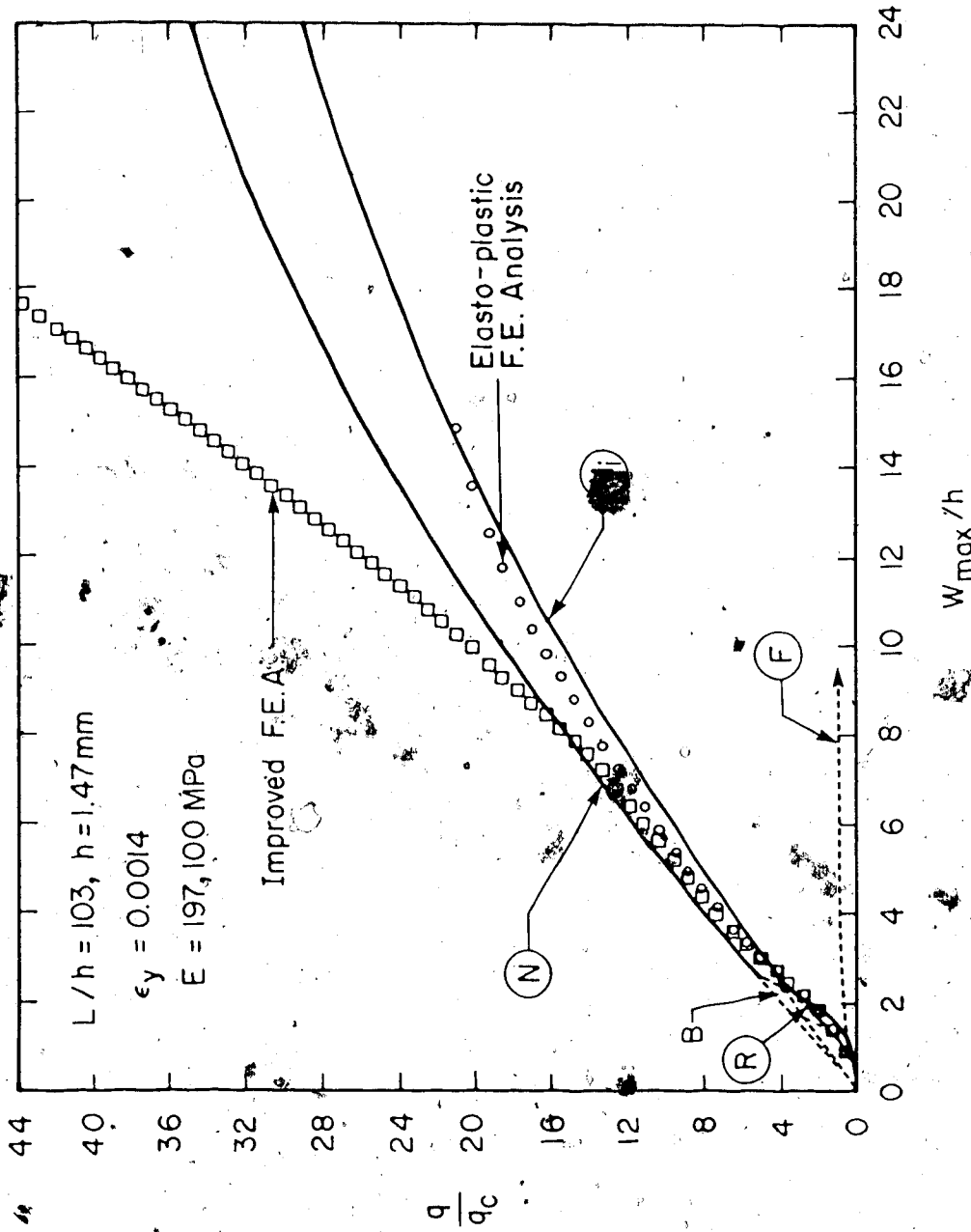
Figure 5.3 Results of finite element analyses

attributed to the fact that, with the bilinear stress-strain

curve assumed, the maximum force developable (at the edge)

is limited to the yield force. Thus with increasing

deflections and therefore increasing edge slope, the

horizontal component of the force in the edge row of

elements and in all other rows of elements must become less.

Considering a free body diagram of one half of the plate

width, L, the rate of increase of the applied load can

decrease when the rate of change of the product of the

increasing maximum deflection and the decreasing horizontal

component of the membrane force decreases. Second, the

finite element curve predicts a gr___ r_de___tion for point

B. In this method, the stiffness m_____ _____rmined for a

giv_n deflection is used to establi___ ___ next increment of

deflection corresp____ ___ to the next increment of load. To

the left of point___ _____use the stiffness of the membrane

is increasing with _____easing deflection, the computational

procedure underestimates the stiffness for the next

increment and hence tends to give larger deflections (this

of course can be somewhat com____sated for by reducing the

load increments).

The elasto-plastic finite element results for the plate

having an L/h of 103 are similar to those found for the

plate with an L/h of 80 but with different material

properties. The elasto-plastic finite element predictions

follow the previously established hypothesis along curve R,

fall below point B, do not rise as high as curve N and

eventually fall below curve M_1. In addition to arguments previously presented, the limited number of elements used through the thickness at the edges may not allow yielding to progress gradually enough through this thickness.

By comparing Figures 5.2 and 5.3 with Figures 3.7 and 3.8, the correspondence between the elasto-plastic finite element analyses and two of Young's test results can be established. The four are in agreement up to point B. Beyond point B, Young's results move to correspond to curve N while the finite element results fall below curves N and M_1 as has been discussed.

5.3 Improved Analysis

A second finite element analysis, identical to that described in section 5.2 but using the linearized stess-strain curve of Fig. 3.5 but now plotted as a true stress-strain curve as shown in Fig. 5.4 to model the material, was used to predict the load-deflection response of a uniformly transversely-loaded plate with L/h equal to 103 and zero aspect ratio. To accommodate the use of a true stress-strain material model and large plate displacements, an updated Lagrangian formulation was used in this analysis. Fig. 5.3 shows the resulting nondimensional load-deflection curve and also the results of the simpler elasto-plastic finite element analysis.

In Fig. 5.5 is shown the deflected two-dimensional through-thickness mesh from this analysis when the
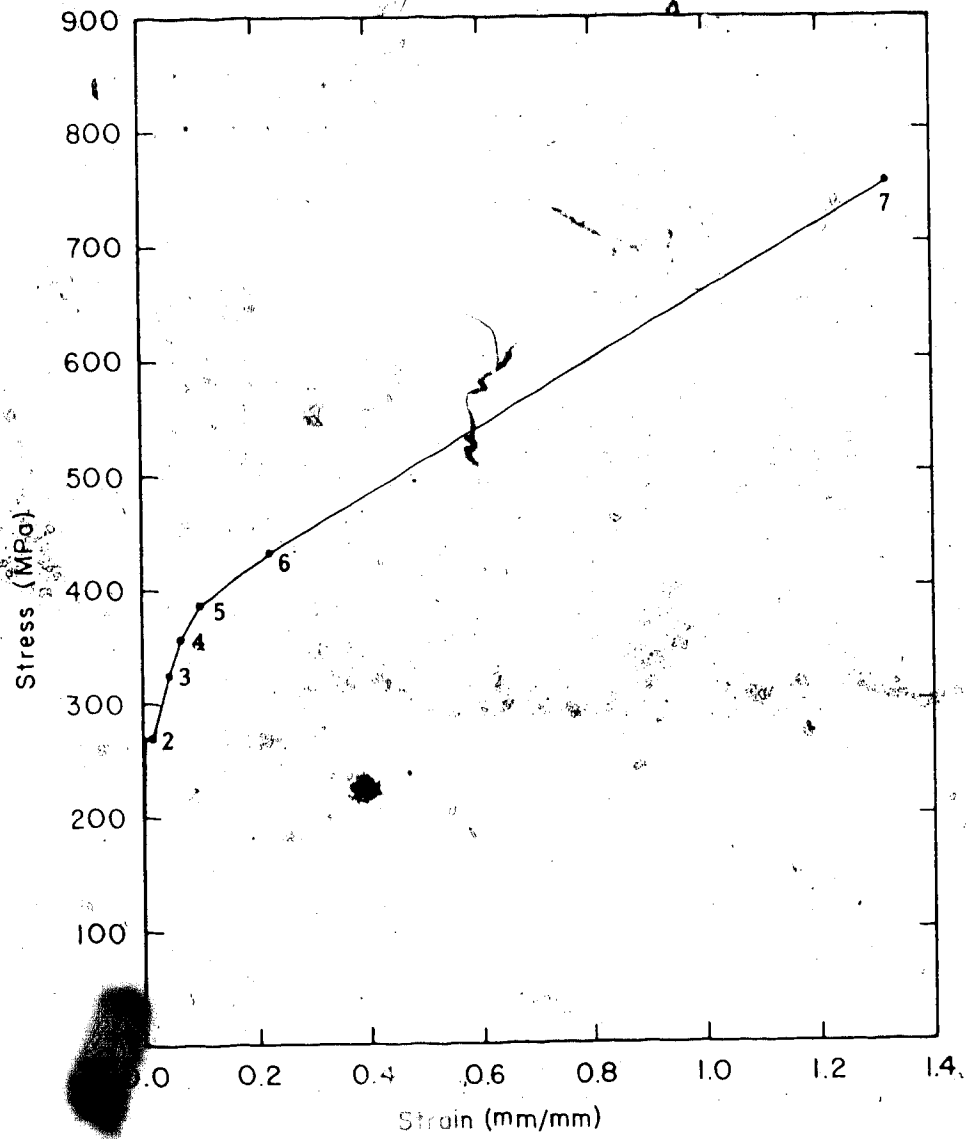
Figure 5.4 Uniaxial true stress-strain curve used in improved finite element analysis
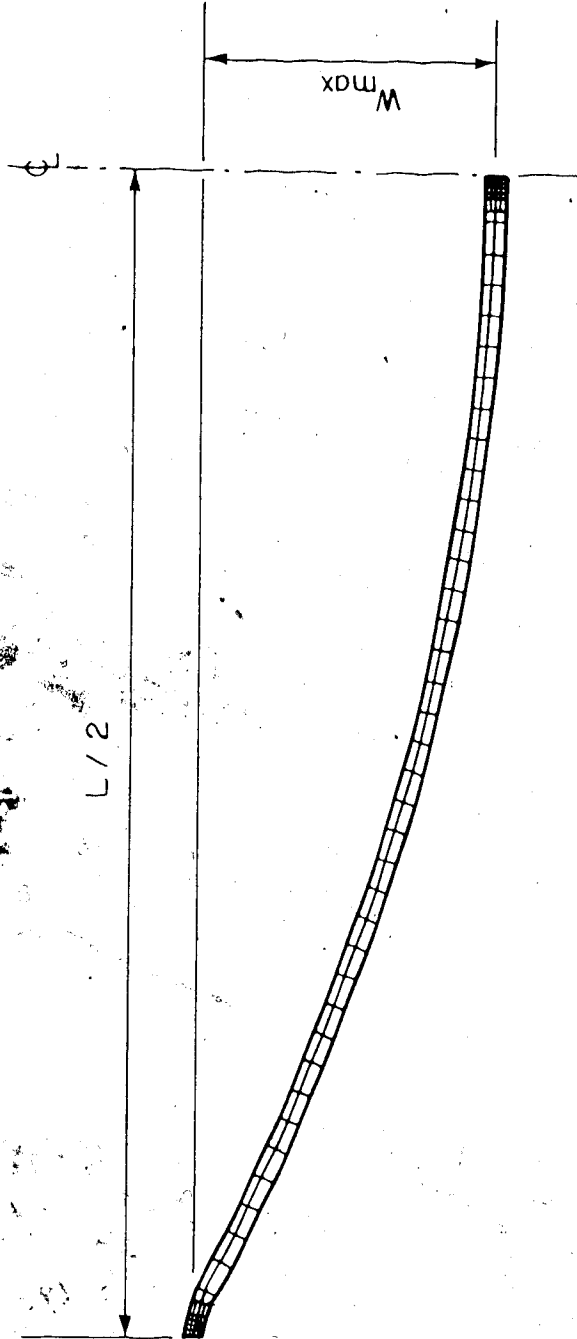
Figure 5.5 Deflected finite element mesh at $q/q = 30$

nondimensional uniform transverse load is equal to 30. From
Fig. 5.3 it is seen that the improved analysis gives a
load-deflection curve beyond point B that lies considerably
above that for the elasto-plastic analysis. The curve also
climbs above curve N as the analysis allows the tensile
stress at the edge of the plate to exceed the yield stress.
The improved analysis therefore confirms the hypothesis
that, with strain-hardening of the material, the load-
deflection behaviour exceeds curve N which is based on a
maximum membrane force equal to the yield force and an
effective inelastic Poisson's ratio of 0.5.

Examining the results of this analysis suggests that
some refinement of the mesh is in order. At the centreline
the refined mesh was used because in early stages of loading
before membrane action developes significant bending moments
exist there. At the edge, however, as established in the
section on local bending and as corroborated by test, a
severe strain gradient exists through the thickness. The use
of even more than 4 layers of elements in this location and
extending to about 2% of the span from the edge would be in
order.

6. EXPERIMENTAL PROGRAM

6.1 General

To verify the various hypothesis put forward, and as pilot tests for large scale tests to follow, two tests were conducted on 1.47 mm thick hot-rolled steel plates 152 mm wide and 456 mm long, having a width to thickness ratio, L/h, of 103 and an aspect ratio of 1/3. The tests were conducted at room temperature, approximately 20 C. With this aspect ratio the central portion of the plate panel should be in a uniaxial plane strain condition with zero strain in the long direction and zero stress through the thickness. The plates were fully restrained on all four sides against rotation and translation and were subject to fluid pressure.

6.2 Test Set-up and Procedure

Fig. 6.1 shows a partial cross-section of the test set-up. The 16 mm diameter bolts were ▮▮▮▮ghtened. Translational resistance at the edges of the specimen was provided by spot-welding the 6 mm x 6 mm bar to the test plate. Silicone sealant spread below this restraining bar and between the specimen and the 25 mm thick base plate provided an effective seal. The base plate and specimen make up a self-contained loading system.

Fluid pressure was monitored by a pressure transducer online between the test set-up and the hand actuated pump. Deflections of the test plate normal to the original surface

16mm A325 bolt at 46 mm spacing

25 mm steel plate

1.47 mm plate specimen

Hydraulic oil under pressure

Oil inlet

6 mm x 6 mm steel bar
resistance welded to specimen

25 mm steel plate

6 mm cavity

Epoxy seal
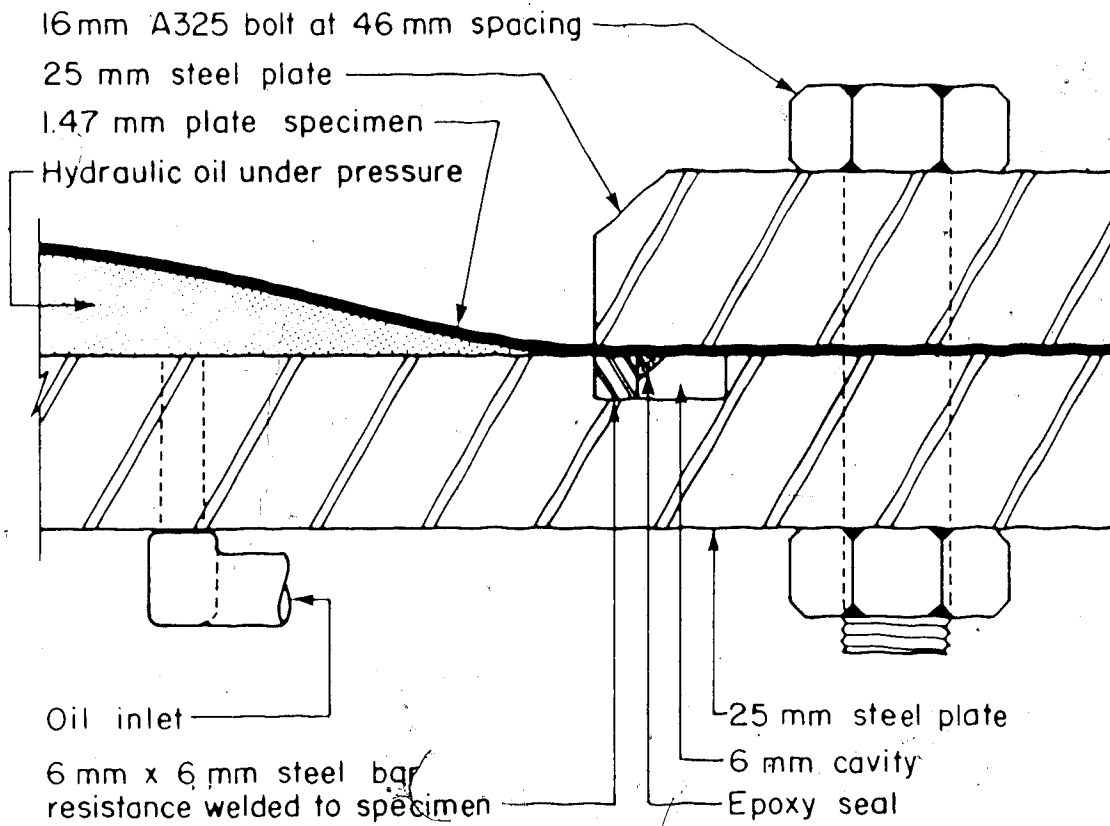
Figure 6.1 Partial cross-section of test apparatus

were measured at several locations using LVDT's (linearly variable displacement transducers) that were calibrated just prior to testing. Fig. 6.2 shows the calibration curves with a central linear range. Electrical resistance strain gauges were mounted on both the inner and outer surface of the test plate. The locations of these gauges and the LVDT's for both tests are shown in Fig. 6.3 and Fig. 6.4. Several of the strain gauges, particularly those mounted across the width of the central portion of the plate were capable of measuring strains in excess of 20%. The lead wires for strain gauges mounted on the inner surface of the specimen were lead through a conical hole in the base plate which was then filled with epoxy resin. This proved effective and no leakage occurred here. All data were recorded using a data acquisition system through which the signals are conditioned, converted from analog to digital form and stored on disk or tape. With this recording equipment a large number of virtually simultaneous readings were taken.

6.3 Ancillary Tests

Six plate coupons with a width of about 30 mm, the full plate thickness of 1.47 mm and a gauge length of 75 mm were tested in uniaxial tension to determine the stress-strain characterisitics of the steel plate. A typical stress-strain curve for a coupon taken parallel to the width of the plate test specimen is given in Fig. 3.5. Table 6.1 gives statistical data from 4 such tests. The other two tests were
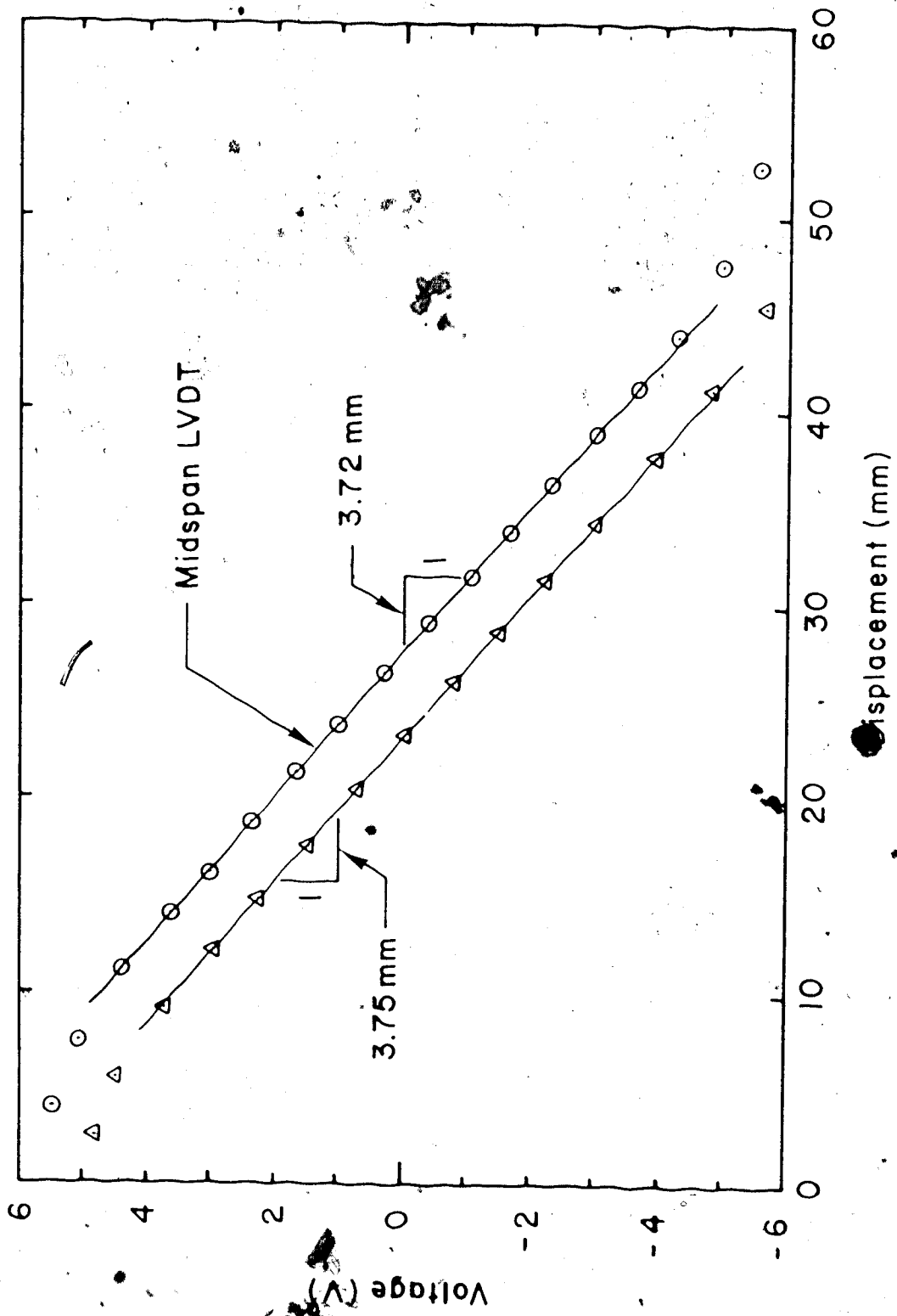
Figure 6.2 LVDT calibration curves

81
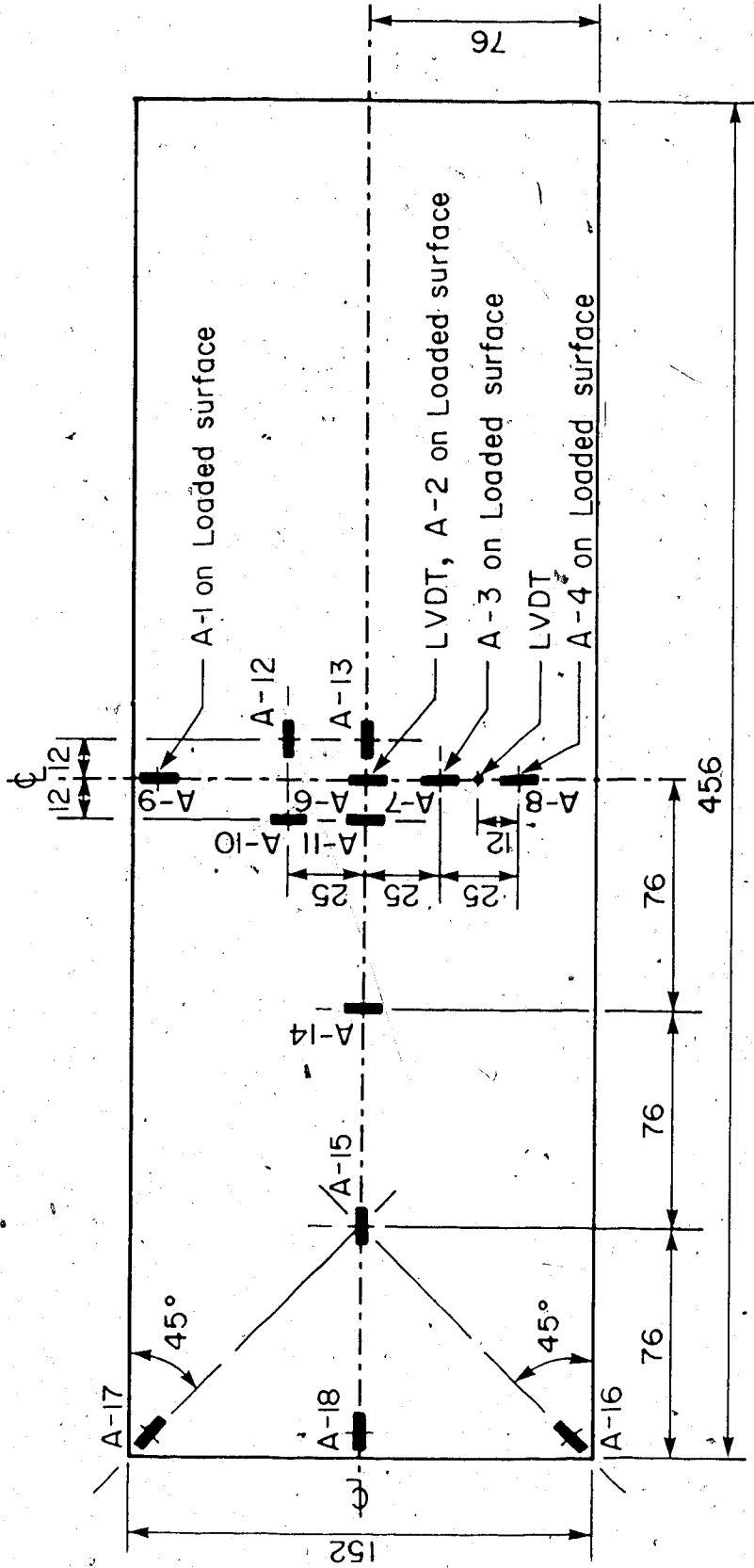
Figure 6.3 Strain gauge and LVDT locations in test-1
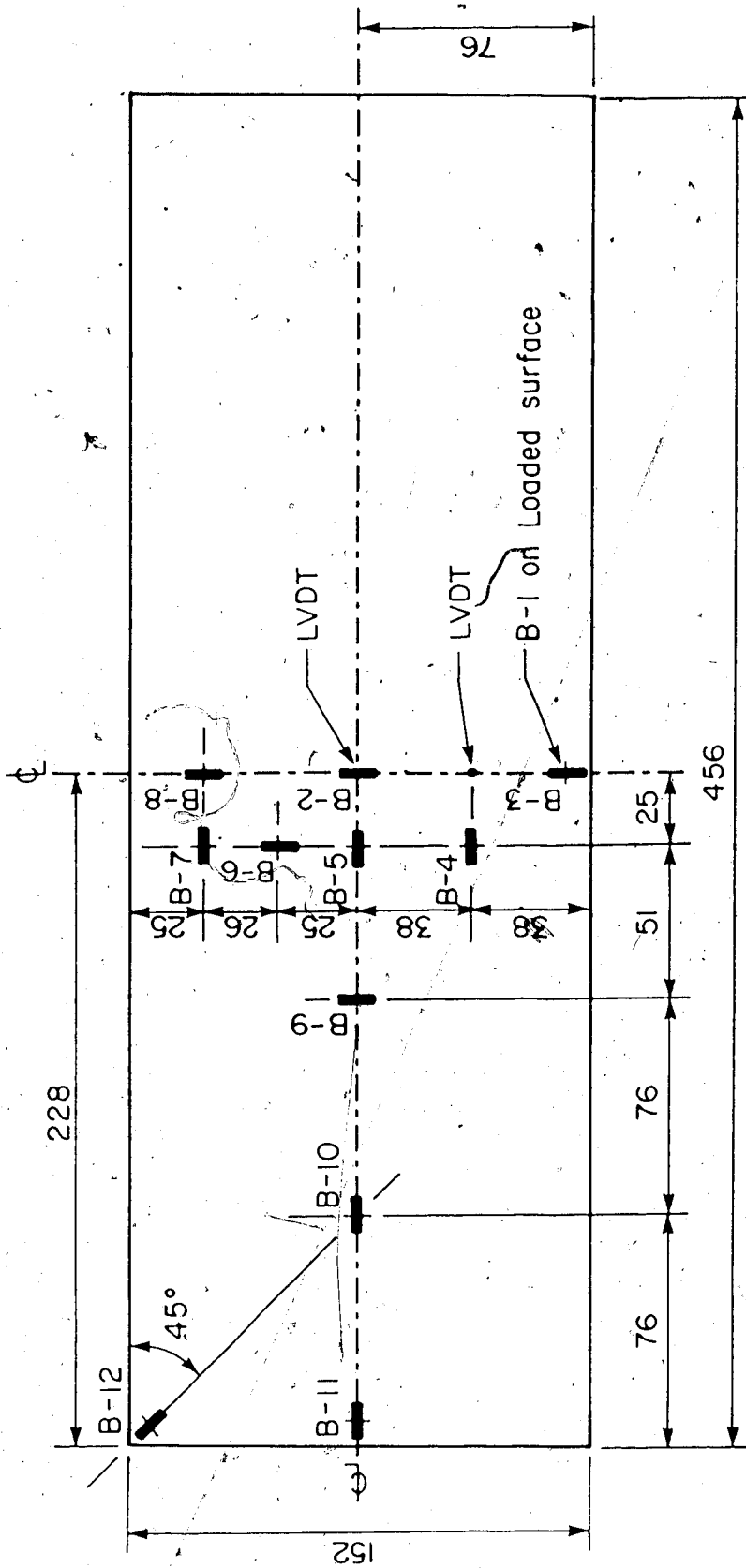
Figure 6.4 Strain gauge and LVDT locations in test 2

done on coupons cut perpendicular to the plate width.

Table 6.1   Tensile coupon test results

Test	E	σ_y	ϵ_{st}	ϵ_f
1	203,100	279	0.018	0.36
2	192,800	264	0.017	0.26
3	201,600	266	0.016	0.31
4	191,000	272	0.018	0.26
Mean	197,100	270	0.017	0.30
V	0.031	0.025	0.019	0.016

To establish local straining charateristics, for use in the local bending analysis and where the test plate is heavily strained, a tensile coupon 1.47 mm thick by 29.15 mm wide was loaded to failure and the strain at failure measured over a series of gauge lengths varying from 100 to 5 mm. The cross-sectional dimensions of the failed specimen at the failure location were 0.51 mm thick and 22.8 mm wide. The variation of fracture strain with gauge length is given in Fig. 6.5 and fitting a ninth order polynomial to the curve gives a maximum strain when extrapolated to zero gauge length of 139%. McGregor (1940) verified by test that the true or natural strain is
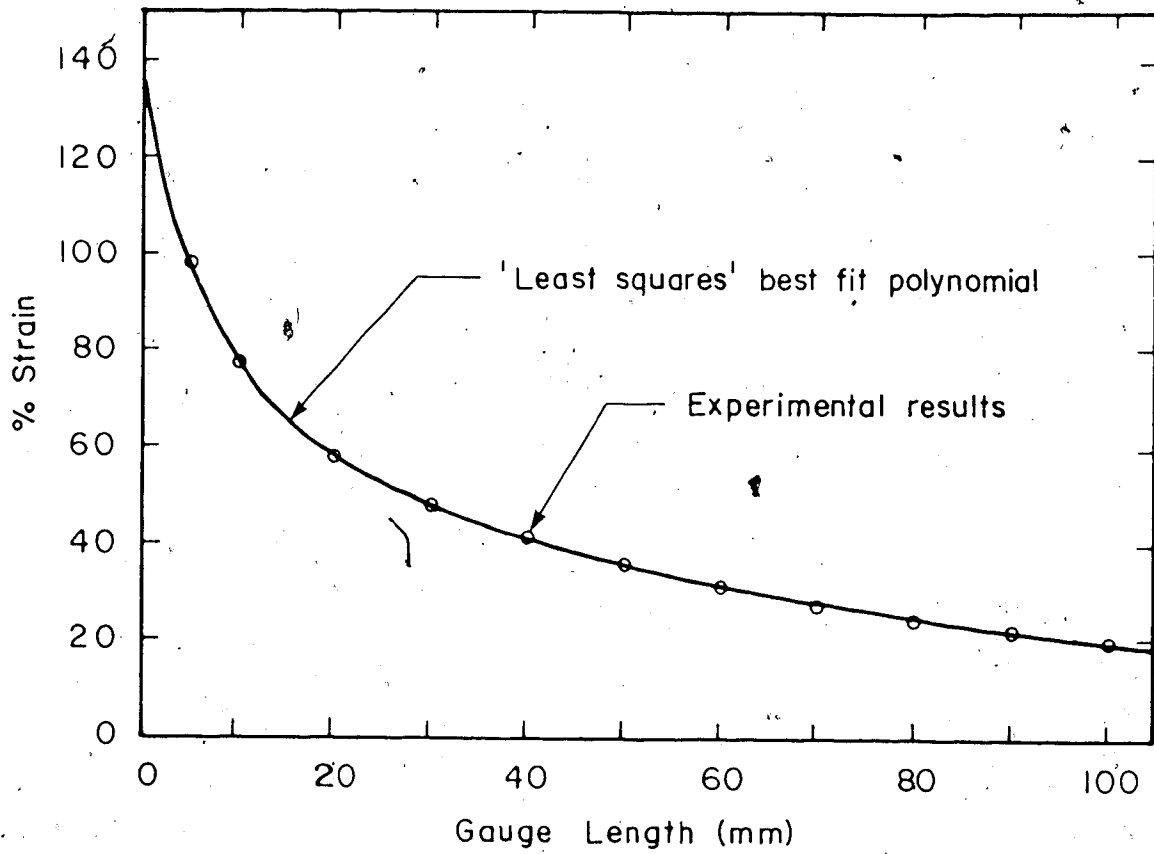
Figure 6.5 Variation of fracture strain with gauge length

$$[6.1] \qquad \epsilon_i = \ell n \ (A_o/A_i)$$

Hosford and Caddell (1983) suggest that the maximum strain in a plate under biaxial tension (as is the case here) is equal to the natural strain at failure:

$$[6.2] \qquad \epsilon_f = \ell n \ (A_o/A_f)$$

By using [6.2] with the test measurements, the failure strain is calculated to be 131%. This is in good agreement with the result obtained by the extrapolation in Fig. 6.5 and is considered to be the more valid result. The ratio of the change in thickness of the tensile coupon at the fracture location to the original thickness divided by the longitudinal strain of 1.31 gives a value for Poisson's ratio at failure of 0.50.

6.4 Test Behaviour and Observations

6.4.1 Overall Behaviour

In Fig. 6.6 are plotted load-deflection curves for the two tests nondimensionalized by dividing the deflection by the plate thickness and by dividing the pressure by the
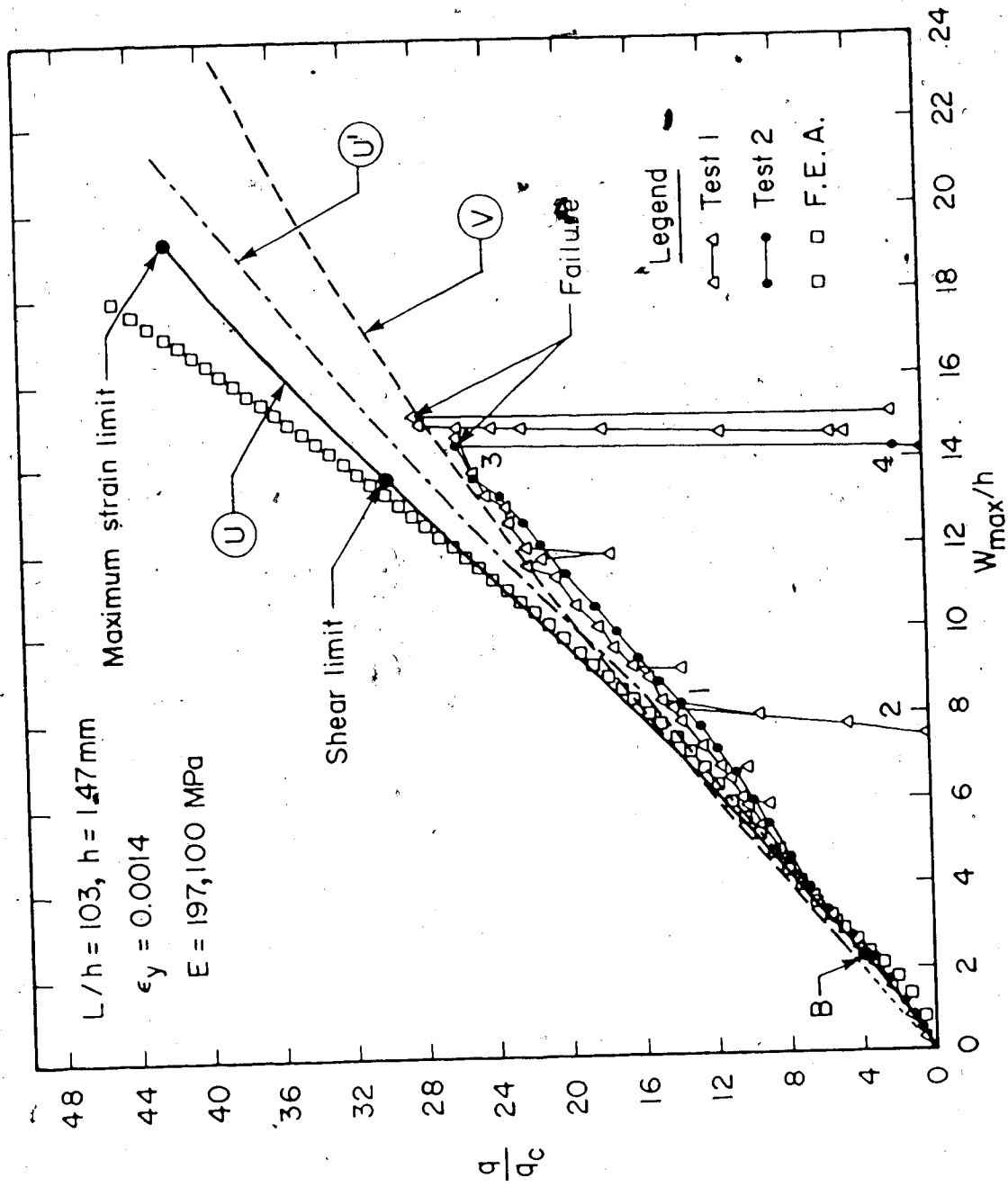
Figure 6.6 Test and predicted load-deflection curves

transverse load per unit area causing a plastic mechanism to form in a similar plate with zero aspect ratio. Although test 2 failed at a lower load than test 1, both load-deflection responses are in good agreement.

On four occasions during test 1, oil was observed leaking from the test set-up. At these times, corresponding to a W_{max}/h of approximately 8, 9, 12 and 15, the load was reduced or removed and the bolts were further tightened. Upon removal of the load, no noticeable decrease in deflections was observed and the plate appeared to retain its "pillow-like" shape. When the fluid pressure was reapplied the load-deflection response traced in reverse the unloading behaviour until the previous maximum load had been reached. Increased loading resulted in a load-deflection behaviour that was simply an extension of that found prior to unloading. The load-deflection behaviour between points 1 and 2 in Fig. 6.5 illustrates the case where the pressure was completely removed and then reapplied. In test 2 the bolts were initially tightened substantially more than in test 1 and no oil leaks were observed. Each of the tests were conducted over a period of approximately 4 hours.

For both tests, plate deformations became visually apparent soon after a nondimensional deflection of about 8 had been exceeded. The bulging of the plate specimens was considerable at the higher load levels. Fig. 6.7, a photograph of the test set-up just after the plate in test 1 failed, shows the "pillowing" effect. At failure, oil

Figure 6.7 Test 1 after failure

spurted out over a length of about 80 mm at the edge along the mid-length of one of the long sides. Subsequent examination revealed that the plate had been sheared in this location. Fig. 6.8, an end-on view of the failed plate of test 1 shows the large deflections that have occurred. The maximum deflection is approximately one-sixth of the span. In the four corners, reverse curvature occurs and is most pronounced on a 45 line running through the corner. Examination of specimen 2 after failure showed that some of the spot welds fastening the plate to the restraining bar had failed. In effect therefore specimen 2 did not fail, but rather the restraining device. Measurements of the cross-section at the middle of the long edges, after failure, for both tests showed that the local flexural and shear deformations there were about equal to the plate thickness. These deflections are those between the edge and point A on Fig. 4.2.

6.4.2 Gauge Measurements

The specimen in test 1 failed at a nondimensional load of 28.6 and a nondimensional deflection of 15.1, equivalent to a fluid pressure of 3850 kPa and a deflection of 22.2 mm respectively. In test 2, when the restraining device failed the maximum nondimensional load and deformation were 25.9 and 14.1 respectively which are equivalent to 3490 kPa and 21.1 mm. Fig. 6.6 shows that the two tests have load-deflection curves that agree closely.
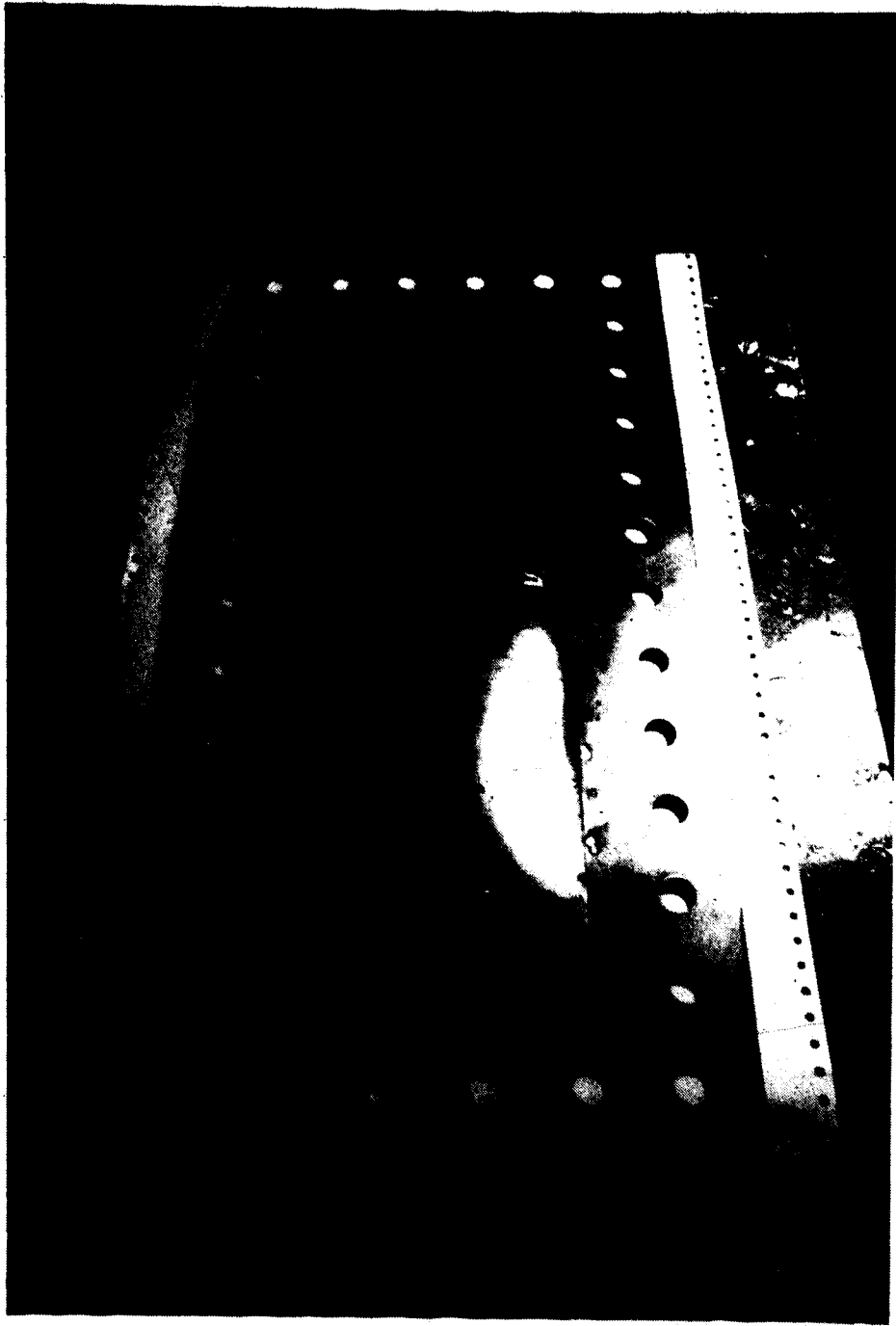
Figure 6.8 Failed specimen of Test 1

In both tests a number of electrical resistance strain gauges were mounted on the steel plate specimen to determine the variation of strain during loading. Gauges A-1, A-2, A-3, A-4, A-6, A-7, A-8 and A-9 of test 1 and gauges B-1, B-2, B-3, B-6, B-8, and B-9 of test 2, located as shown in Fig. 6.3 and Fig. 6.4 respectively, measured strains across the width and were located within the central third of the plate length. The load-strain response of these gauges is shown in Fig. 6.9, Fig. 6.10 and Fig. 6.11. The general behaviour of these gauges is the same although the initial rate of change of strain with load for gauges A-1, A-2, A-3 and A-4 is less than that for the remainder. Beyond a nondimensional load of approximately 8 the strain in all the gauges increases rapidly at a similar rate. The strains at a nondimensional load level of 8 correspond to strains in the yield plateau ($\epsilon_y \; \epsilon \; \epsilon_{st}$) as may be determined from Fig.6.9, Fig. 6.10 and Fig. 6.11. It would be expected that with yielding the strains would tend to increase much more rapidly with load. From Fig. 6.6 it is seen that at a load level of about 8 the nondimensionalized deflection value based on curve U of slightly greater than 4 lies between point B where the membrane is just fully yielded in tension and the point, $W_{max}/h = 8.2$, corresponding to the attainment of the strain-hardening strain. Before reaching the yield plateau the rate of increase of strains exhibited by gauges mounted on the loaded side is much less than for gauges mounted on the unloaded side as can be seen by comparing
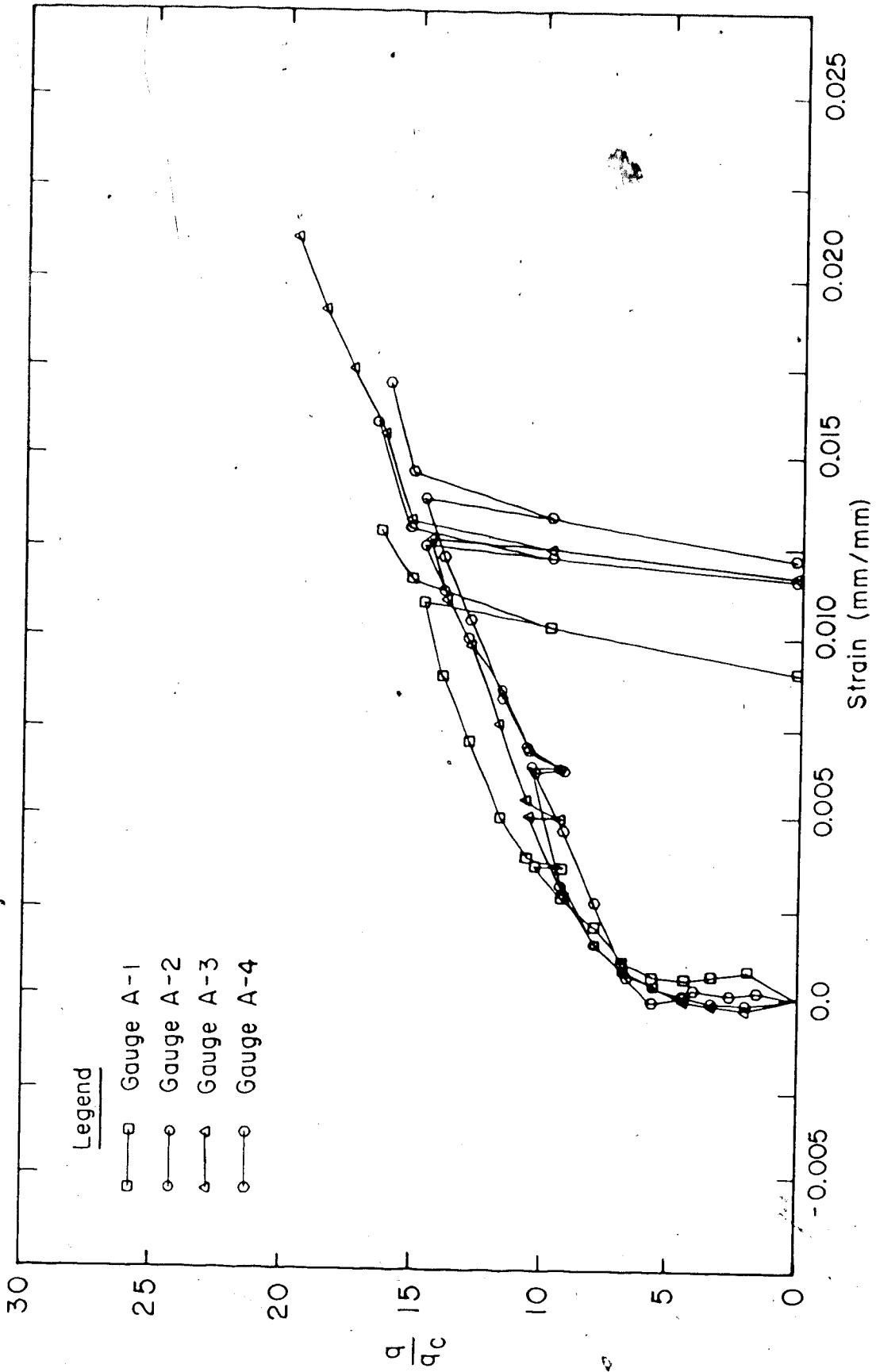
Figure 6.9 Test 1 strain gauge results
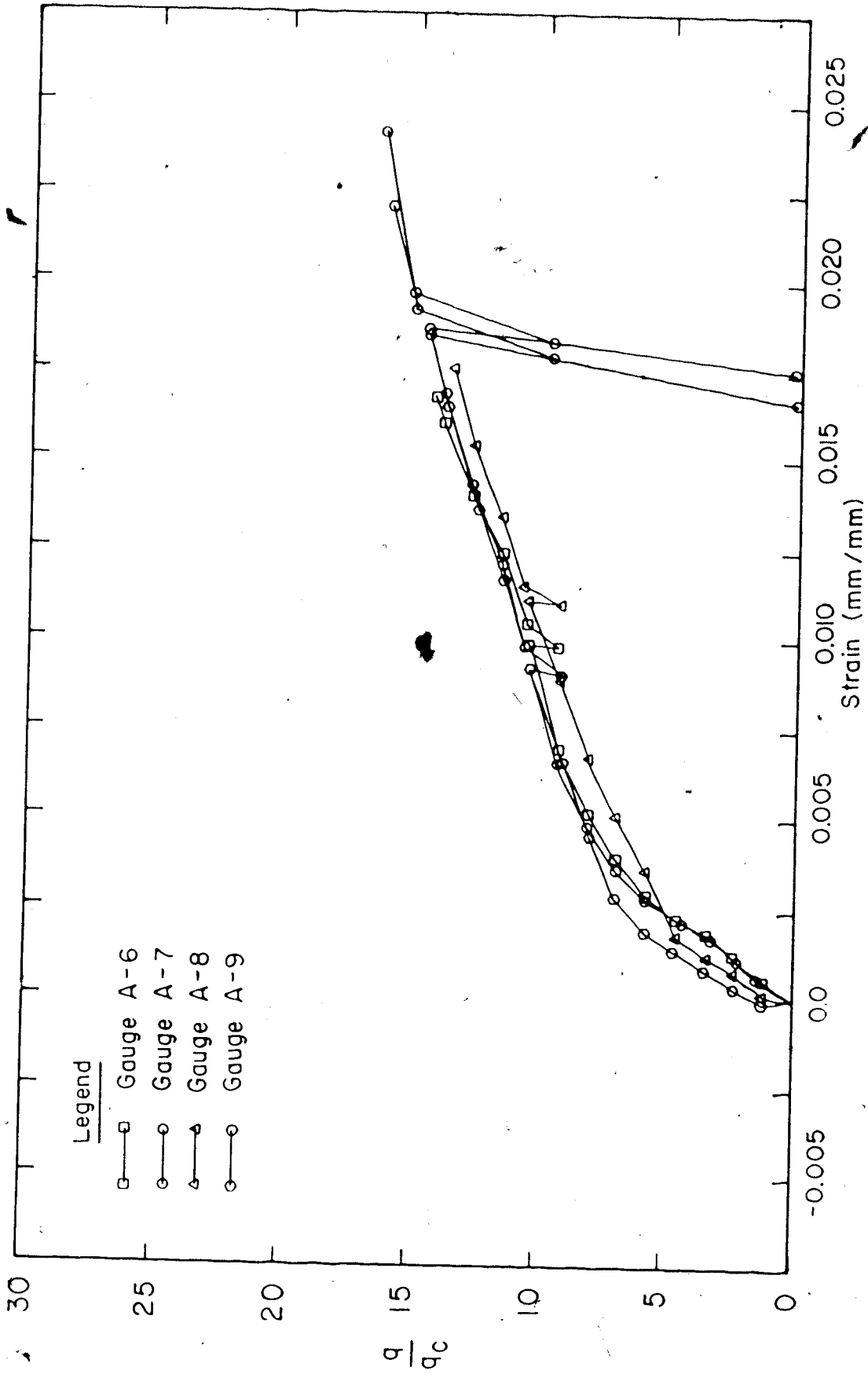
Figure 6.10 Test 1 strain gauge results
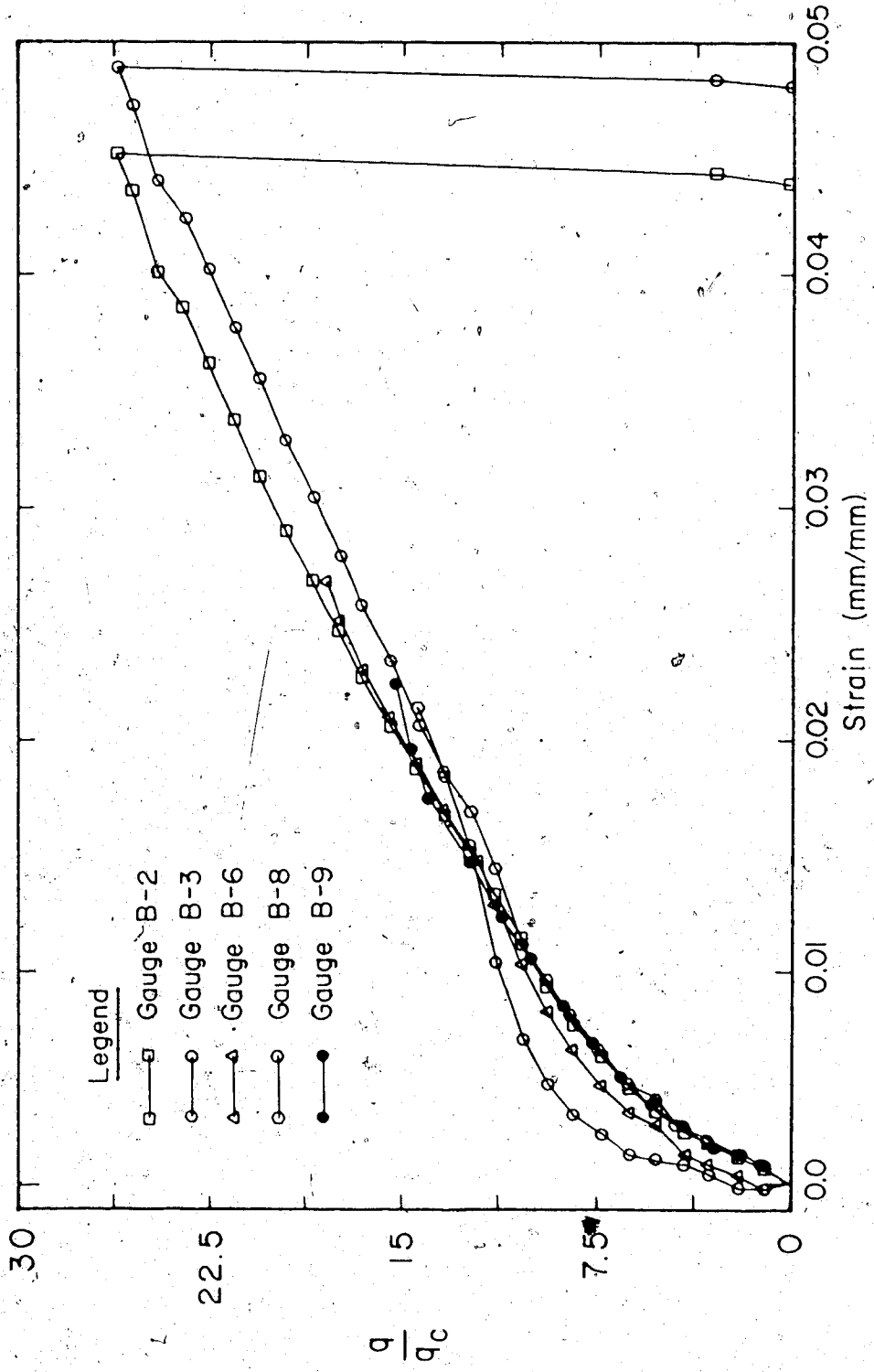
Figure 6.11 Test 2 strain gauge results

Fig. 6.9 to Fig. 6.10 and Fig. 6.11. The reason for this is not apparent.

From Fig. 6.6 the nondimensionalized load when strain-hardening is reached (ϵ_{st} = 0.017) is 16.2. Based on the geometry of the test and this mean value of the strain at the mid-thickness of the plate, the strain on the outside surface would be 0.0201 and that on the inner surface, 0.0140. From Fig. 6.9 and 6.10, the outer surface strains at this load level are determined on the average to be 0.023 and the inner surface strains 0.015. These measured strains are in reasonable agreement with those predicted from the geometry and serve to confirm that the plate is being deformed into a circular shape. In the first test, the gauges A in Fig. 6.9 and 6.10 generally failed at about the onset of strain-hardening. In the second test where some high-elongation gauges were used, as shown in Fig. 6.11, strains in the gauges continue to increase at about the same rate beyond the beginning of strain-hardening as before.

The average maximum strain recorded in test 2 (gauge B-2 and B-3) at a nondimensionalized load of 25.9 was 0.047. The computed nondimensionalized deflection for this strain is 13.8 whereas that measured as shown in Fig. 6.6 was 14.1. These are in reasonable agreement.

A basic assumption of the analyses presented is that the central one-third of the test specimens would be subjected to a uniaxial plane strain condition, that is, that the longitudinal strains would be zero. From Fig. 6.12,
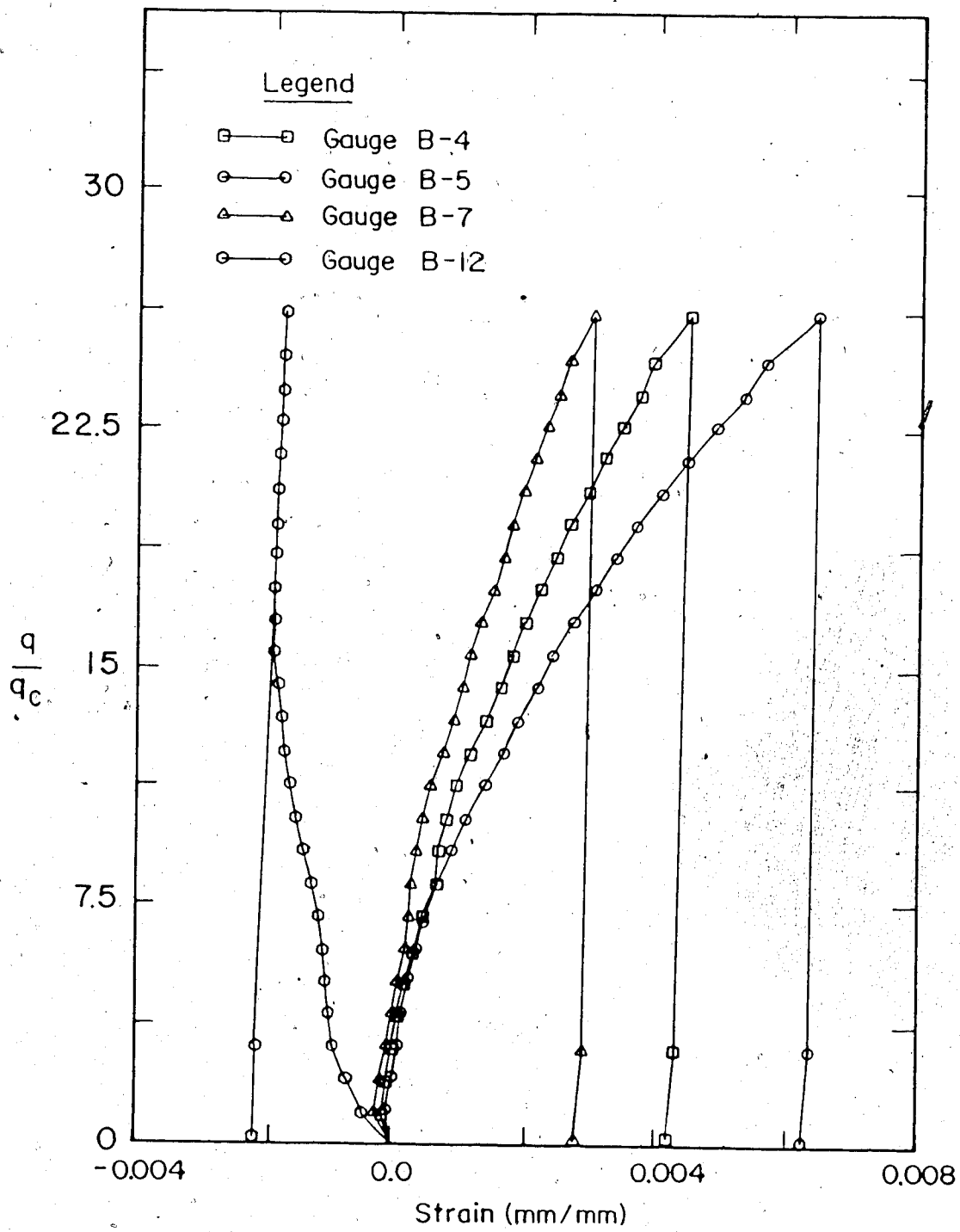
Figure 6.12 Test 2 strain gauge results

longitudinal gauges B-4, B-5 and B-7 indicate on the average a tensile strain, at the nondimensionalized failure load of 25.9, of 0.045. These strains are about 9.7% of the strains in the transverse direction and indicate that not only is the plate being prevented from contracting in the longitudinal direction (the Poisson effect) but that tensile strains are being developed longitudinally and therefore that some load is being carried in that direction.

The results of the strain readings of gauge B-12 given in Fig. 6.12 are typical of those gauges mounted on the unloaded face in the corners at 45° to the long axis of the specimen. Compressive strains existed there throughout the test, consistent with the concave upward curvature present in the corners.

6.5 Comparisons of Results with Analytical Predictions

6.5.1 Membrane and Ultimate Strength Analyses

Curve U in Fig. 6.5 gives the predicted load-deflection curve based on the complete stress-strain curve of the material to failure. On this curve are marked the limiting loads as determined by the maximum strain and shear criteria. For this plate the lower value of nondimensional load of 29.5 (shear limit), equivalent to 3960 kPa, governs and gives a test to predicted ratio of 0.97 for test 1. Comparing the predicted maximum deflections by curve U with the values of both tests in the upper ranges gives a test to

predicted ratio of 1.16. Curve U does not however take into account the flexural and shear deformations that occur adjacent to the edges. Curve U' shown in Fig. 6.6 is derived from curve U to take the observed edge deformation into account based on the assumption that this deformation, observed to be equal to the thickness of the plate, is proportional to the transverse load. Using the corrected curve U', the ratio of the test to predicted deflections near failure is 1.08.

6.5.2 Finite Element Analysis

The results of the finite element analysis (F.E.A.) based on the linearized stress-strain curve are plotted in Fig. 6.6 along with the test results. This curve although drawn for a uniform lateral pressure corroborates reasonably well the test results for the plate loaded with fluid pressure. At a nondimensional load of 28 the F.E.A. deflection is only 85% of the value of test 1. Although not definitely established the reason for the increased stiffness of the F.E.A. appears to be associated with the boundary conditions of the model. Up to the shear limit the F.E.A. results do however follow quite closely the simple analysis of curve U based on the stress-strain curve beyond strain-hardening. In particular, the F.E.A. shows the same kink in the load-deflection behaviour at the predicted onset of strain-hardening at a W_{max}/h approximately equal to 8.2. The F.E.A. failure criterion was a maximum strain of 1.32

and the curve terminates close to the maximum strain limit
of curve U. No shear criterion limit was modelled in the
F.E.A.

6.5.3 Deformations

After the failure in test 2, the edge slope of the
plate at the mid-length of the long sides was measured to be
31. Edge slopes of 29.3° and 30.5° were determined from the
local bending analysis corresponding to strain measurements
from gauges B-2 and B-3 of 0.045 and 0.049 taken just prior
to failure. These strain measurements therefore confirm
those predicted by the local bending analysis.

The deflection measurements provided by the 2 LVDT's
confirmed within 2%, under fluid pressure loading, (when the
central portion of the plate is behaving essentially as an
inelastic membrane) that the shape across the width at the
middle of the long sides is circular.

6.6 Summary

The load-deflection curves for the two tests agree
closely. The membrane analysis taking into account the
portion of the stress-strain curve beyond the beginning of
strain-hardening is in good agreement with the test results.
For this plate the shear failure criterion governs and gives
a test-to-predicted load ratio of 0.97. By taking into
account the flexural and shear deformations at the edge the
ratio of test-to-predicted deflection at failure is 1.08.

The maximum deflection at failure was found to be greater
than one-sixth of the plate width.

The results of the F.E.A. based on the linearized
complete stress-strain curve follow closely the simple
analysis of curve U also based on the stress-strain curve
beyond strain-hardening. The maximum load predicted by the
F.E.A. based on an ultimate local strain of 1.32 was close
to the maximum strain failure limit of curve U based on the
same strain. No shear criterion was modelled. At the onset
of strain-hardening, the F.E.A. shows the same kink in the
load-deflection behaviour at W_{max}/h equal to 8.2 as shown by
the test results and the inelastic membrane curve U.

Strain gauges within the central third of the length of
the plate that measured strains across the width exhibited
similar behaviour. Relatively small longitudinal strain
measurements were recorded. Predicted edge slopes of the
plate at the middle of the long sides at failure were in
good agreement with those obtained from strain measurements.

Prior to failure, unloading results in a near elastic
load-deflection path that is retraced upon reloading until a
load greater than that acting prior to unloading acts.

7. DESIGN APPLICATION

It appears that the full strength of continuous steel plates loaded transversely could be utilized in designing offshore oil exploration and production structures for use in the Arctic. Under these circumstances the plates would be designed to carry the factored loads at the ultimate limit state in accordance with the criteria established herein. The plates would be analyzed for whatever distribution of ice loads is considered feasible. A number of other limit states or conditions would have to be examined and, if critical, satisfied. These conditions include the fatigue behaviour, the response under different loading conditions and the anchorage of the plates around the periphery so that the membrane forces can be developed. The designer should also be satisfied that the deflections under service loads would be acceptable.

Assuming that the plate thickness has been selected based on membrane action to sustain the factored transverse loads when the factored resistance, based on either the shear failure criterion or the maximum strain criterion, has been reached, the designer would check the deflections at specified load levels. These deflections are expected to be appreciable and must be considered to be acceptable for the intended structure. For the plates tested, with a width to thickness ratio of about 100, the maximum deflection at ultimate load was approximately one-sixth of the width. Assuming that the load factor consistent with the maximum

load was, say, 1.5, from Fig. 6.6 the deflection corresponding to the specified load is determined to be about one-tenth of the span. It is suggested that deflections of this order of magnitude would be acceptable for offshore oil exploration and production structures in the Arctic. The structure would have the safety level required and the deflections would not affect its serviceability. In determining the strength of the supporting frames or ribs, the deflected shape of the plate as shown in Fig. 7.1 would of course have to be taken into account.

To examine the question of fatigue loading consider the load-deformation response of Fig. 6.6. Points 1 to 2 and points 3 to 4 show the behaviour of the membrane on unloading. On reloading these paths are retraced. If a certain load, say that represented by point 1 has been reached and then removed, further cycles of loading to the same or a lesser level would simply cause cycling between points 2 and 1. If on the other hand the maximum load on a subsequent cycle was intermediate to points 1 and 3, cycling would occur on a line through this point at about the same slope as the line joining points 1 and 2. It is anticipated that a significant number of cycles of loading displaying this essentially elastic behaviour could be withstood before fatigue cracking would ensue. It is further anticipated that the number of cycles of extreme loading that a caisson type structure used for oil production in the Arctic, when

Box beam at periphery

Ribs

Deformed plate panel
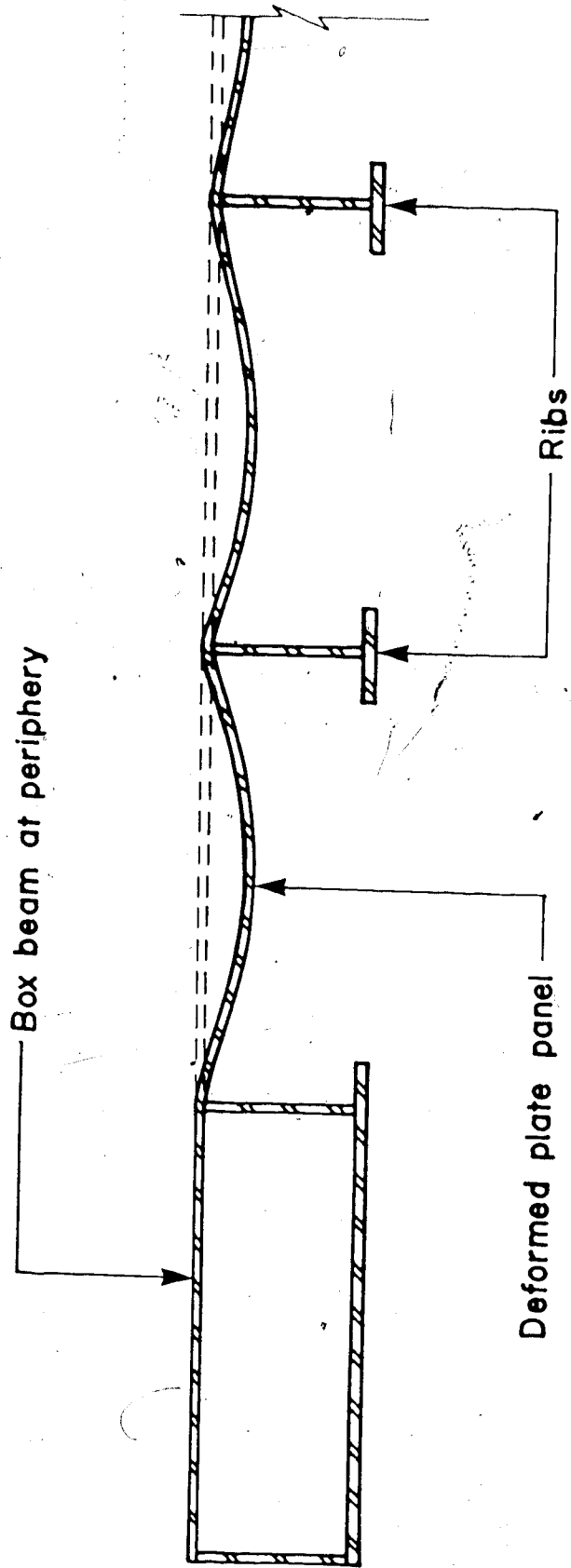
Figure 7.1 Proposed restraint at structure periphery

designed at ultimate against ice forces with a return period of, say, 100 years, would not be sufficient to cause fatigue failure.

The deflected shape of an individual plate panel is directly related to the distribution of loads to which it has been subjected. If, therefore, a panel is subjected to a loading pattern different from that which first occurred, a new inelastic deflected shape would be developed as shown by McDermott et al. (1974) provided the second load is sufficiently large. The panel simply adapts to the new loading conditions. The variation in loading on a panel is therefore seen not to be a problem. As a matter of fact the permanent deformations that have occured can be used directly to determine the intensity of the forces to which plate panels of the structure have been subjected. The structure itself becomes a conglomeration of virtually indestructable ice load measuring devices. The deflected shapes provide a significant clue to the distribution of load. Therefore, when subject to ice forces, the steel plates forming the skin of a caisson type structure would act as load measuring devices. It would be necessary only to record the deflected shapes. Yearly observations would enable the operator to catalogue the forces to which the structure has been subjected, thus accumulating a body of statistical data.

The total transverse load applied to the steel plates or panels must eventually be transferred by the supporting

ribs and framing members to the ground. These members therefore must sustain the loads as they would in a more conventional design. The membrane behaviour requires, in addition, that the tensile forces developed in the panel be anchored around the periphery of a series of panels. Such anchorage can be provided by framing members acting in the plane of the plate. One solution that appears feasible would be to form box beams around the periphery as shown in Fig. 7.1. The tensile membrane forces subject the box beams to lateral bending moments and considering the tensile forces developed in the orthogonal direction the box beams would also be subject to compressive forces.

To utilize the ultimate capacity of plates, i.e. the inelastic membrane action, implies that such behaviour will occur at the low ambient temperatures that can be expected in the Arctic. While the plates are subject to extensive straining they are relatively thin and should not have significant discontinuities or stress raisers. Tests of plates under cold temperatures would delineate the suitability of currently available steels in this application.

The use of the full strength of continuous steel plates as developed with inelastic membrane action has further applications in any circumstances where the significant deformations that do develop are not of importance. Other applications could include structures for storing materials such as tanks, bins and hoppers.

8. SUMMARY AND CONCLUSIONS

8.1 Summary and Conclusions

1. An extensive literature search has not revealed that satisfactory solutions exist for the load-deflection response of transversely loaded continuous steel plates beyond the elastic limit when taking into account both flexural and membrane action. Many elastic solutions for the load-deflection response of plates having varying aspect ratios are available. Some inelastic solutions of limited appplicability are also available. The inelastic solutions, extensions of Timoshenko's (1940) elastic solution, include those of Clarkson (1956), Chien and Yeh (1956) and Hooke (1969,1970), among others, and are either closed-form or iterative.

2. Experimental data, limited in the inelastic range of behaviour, show that the elastic solutions for the load-deflection response of plates of any aspect ratio can be considered valid to the point where a fully plastic hinge in the presence of axial force has formed at the edges of the plate. Without considering strain-hardening, this finding validates the assumption of using a bilinear moment-curvature relationship to model the flexural behaviour of a steel plate.

3. By considering relationships describing limiting behavioural modes of transversely loaded continuous steel plates, the domain in which the load-deflection response lies is established. The first portion of the domain governs the behaviour until full yielding occurs in tension along the long edges. The second portion, governing the behaviour when inelastic membrane action occurs, is based on an elasto-plastic stress-strain relationship. Within this domain the plate first behaves in a combined flexural membrane mode, until plastic hinges form at the edges of the long sides. This hinge formation results in decreased stiffness. With further loading flexural membrane action continues but flexural action is eventually obliterated when the entire cross-section is yielded in tension. Additional transverse load can then be applied to the plate as deflections increase due to increased axial straining. The analysis, verified by test, predicts the behaviour to the point where the membrane is fully yielded in tension. Beyond this point, the analysis gives the domain in which the load-deflection response lies, as Poisson's ratio increases from the elastic to the inelastic value and strains greater than the strain-hardening strain develop in the membrane. The analysis, as substantiated by the available experimental results of others and test data reported here, shows that a continuous flat plate subjected to uniform

transverse loads and fluid pressure, when membrane action is considered, can carry a transverse load many times that determined on the basis of flexural action only.

4. An analysis culminating with inelastic membrane behaviour and taking into account the stress-strain curve beyond the beginning of strain-hardening gives a load-deflection response lying within the behavioural domain to the point where the straining beyond the yield strain plays a role.

5. Edge effects, that give rise to local bending and shearing stresses, limit the load that can be carried and increase the deflections slightly. Two failure criteria based on edge effects, one related to maximum tensile straining and the other to shear loading, have been developed.

6. Two finite element analyses have been performed on an infinitely long continuous steel plate model. The first analysis is based on an elasto-plastic stress-strain relationship for the steel and the other considers the complete stress-strain curve to failure. Both analyses follow closely the predicted behaviour to the load corresponding to complete yielding of the membrane in tension at the edges. Beyond this the analysis based on

the complete stress-strain curve gives a load-deflection response that corresponds well with the membrane analysis predictions that include strain-hardening and also is in reasonable agreement with the test data. Some modifications to the finite element mesh and to the manner in which the boundaries are modelled is suggested.

7. Two tests were conducted on 1.47 mm thick steel plates with an aspect ratio of 1/3 and a width to thickness ratio of 103. The plates were clamped against rotation and translation at all four edges and subjected to fluid pressure. Edge-shear failure occurred in one plate at a pressure of 3850 kPa, tha is at 28.6 times that of the simple plastic flexural analysis and is 0.97 of that predicted. The average failure deflection is 1.08 times that predicted using the inelastic membrane analysis. In the second test the edge restraint failed. Even when significant inelastic membrane deflections have occurred the unloading and reloading response is nearly elastic.

8. The behaviour, assuming that inelastic membrane action fully predominates, is well substantiated by the tests.

9. Strain measurements taken on the steel plates tested are consistent with the behaviour described herein.

10. It appears that the inelastic membrane strength of continuous steel plates loaded transversely could be utilized in designing the skin plates of caisson-type offshore structures for use in the Arctic. The significant plate deflections that can occur would have to be considered to be acceptable. It is anticipated that a significant number of cycles of loading could be withstood and therefore that fatigue would not be a problem. Changing the loading patterns would not unduely influence the overall behaviour. To utilize the membrane action requires proper design of framing members and steels selected would have to be appropriate for use in the Arctic.

11. When the load-deflection response is known the plates forming the skin of a caisson type structure can be utilized as load measuring devices.

8.2 Areas of Future Work

1. The analyses presented are limited to plates of zero aspect ratio and should be extended to plates with other aspect ratios.

2. A number of refinements to the finite element analyses are suggested. These include increasing the number of elements used near the plate edge and changing the

boundary conditions at the fixed edge to model more closely the real conditions that would exist there. A three-dimensional finite element analysis is recommended for analyzing plates with aspect ratios other than zero.

3. A comprehensive test program on transversely loaded plates with well defined material properties and boundary conditions should be conducted. These tests sho be of substantial scale. Parameters to be investigated include the aspect ratio and the length to thickness ratio.

4. Further knowledge of the behaviour under cyclic loading and the behaviour under low temperature conditions would be valuable.

5. Research is needed to determine the effect of the deflected shape of the plate on the strength and behaviour of supporting frames or ribs.

6. Framing methods need to be developed to ensure that the plates are anchored sufficiently such that they may behave as inelastic members.

REFERENCES

ADINA Engineering Inc., 1981. ADINA Engineering Report AE
    81-1., Massachusetts.

Boobnoff, I.G., 1902. On the Stresses in Ship's Bottom
    Plating Due to Water Pressure. Transactions of the
    Institution of Naval Architecture, 44, p. 15.

Canadian Standards Association, 1984. Steel Structures for
    Buildings - Limit States Design, National Standard of
    Canada CAN3 S16.1-M84. Canadian Standards Association,
    Rexdale, Ontario.

Chien, W.Z., 1947. Large Deflection of a Circular Clamped
    Plate. Chinese Journal of Physics, Shanghai, pp.
    102-113.

Chien W.Z. and Yeh, K.Y., 1957. On the Large Deflection of
    Rectangular Plate. Proceedings of the 9th International
    Congress of Applied Mechanics, Brussels, pp. 403-412.

Clarkson, J., 1956. A New Approach to the Design of Plates
    to Withstand Lateral Pressure. Transactions of the
    Institution of Naval Architecture, 98, pp. 443-463.

Hooke, R., 1969. An Approximate Analysis of the Large
    Deflexion Behaviour of Clamped, Uniformly Loaded,
    Rectangular Plates. Journal of Mechanical Engineering
    Science, 11, pp. 256-268.

Hooke, R., 1970. Post-Elastic Deflection Prediction of
    Plates. Journal of the Structural Division, American
    Society of Civil Engineers, 96 (ST 4), pp. 757-771.

Hooke, R. and Rawlings, B., 1969. An Experimental
    Investigation of the Behaviour of Clamped, Rectangular,
    Mild Steel Plates Subjected to Uniform Pressure Loading.
    Proceedings of the Institution of Civil Engineers, 42,
    pp. 75-103.

Hosford, W.E. and Caddell, R.M., 1983. Metal forming,
     Mechanics and Metallurgy. Prentice Hall Inc., Inglewood
     Cliffs, N.J., 330 pp.

Jones, N., 1971. A Lower Bound to the Static Collapse
     Pressure of a Fully Clamped Rectangular Plate. M.I.T.,
     Department of Ocean Engineering Report 71-20.

Jones, N., 1976. Plastic Behaviour of Ship Structures.
     Presented at the annual meeting of the Society of Naval
     Architects and Marine Engineers, November. pp. 115-145.

Jones, N. and Walters, R.M., 1971. Large Deflections of
     Rectangular Plates. Journal of Ship Research, 15 (2),
     June, pp. 164-171 and p. 288.

Kennedy, D.J.L. and Hafez, M.A., 1984. End Plate Connections
     for Steel Beams. Canadian Journal of Civil Engineering,
     11 (2), pp.139-149.

Kriviak, G.J. and Kennedy, D.J.L., 1985. Standardized
     Flexible End Plate Connections for Steel Beams.
     Proceedings: Canadian Society for Civil Engineering
     Annual Conference, Saskatoon, Saskatchewan, May 27-31,
     pp. 481-501.

Lay, M.G., 1982. Structural Steel Fundamentals. - An
     Engineering and Metallurgical Primer. Australian Road
     Research Board, Nunawading, Victoria, Australia, 241 pp.

Levy, S., 1942. Square Plate With Clamped Edges Under Normal
     Pressure Producing Large Deflections. N.A.C.A. Report
     No. 740.

MacGregor, C.W., 1940. The Tension Test. Symposium on
     Significance of the Tension Test. Proceedings: American
     Society for Testing and Materials, 40, pp. 508-534.

Marguerre, K., 1938. Zur Theorie Der Gekrummten Platte
     Grosser Formanderung. Proceedings of the 5th
     International Congress on Applied Mechanics, Cambridge,
     Massachusetts, pp. 93-101.

McDermott, J.F., Kline, R.G., Jones, Jr., E.L., Manier, E.L., Maniar, N.M. and Chiang, W.P.; 1974. Tanker Structural Analysis for Minor Collisions. Transactions, The Society of Naval Architects and Marine Engineers, 82, pp. 382-414.

Nylander, H., 1951. Initially Deflected Thin Plate with Initial Deflection Affine to Additional Deflection. International Association for Bridge and Structural Engineering, 11, pp. 347-374.

Stang, A.H., Greenspan, M. and Newman, S.B., 1946. Poisson's Ratio of Some Structural Allays for Large Strains. Research Paper RP-1742, Journal of Research of the National Bureau of Standards, 37, October, pp. 211-221.

Timoshenko, S., 1940. Theory of Plates and Shells, 1st. Edition. McGraw-Hill Book Company, London, England.

Timoshenko, S. and Woinowsky-Krieger, S., 1959. Theory of Plates and Shells, 2nd ed. McGraw-Hill Book Company, New York.

Way, S., 1938. Uniformly Loaded, Clamped, Rectangular Plates With Large Deflections. Proceedings of the 5th International Congress of Applied Mechanics, Cambridge, Massachusetts, p.123.

Young, A.G., 1959. Ship Plating Loaded Beyond the Elastic Limit. Transactions of the Institution of Naval Architecture, 10, pp. 143-165.